UNIVERSIDADE DE LISBOA
FACULDADE DE CIÊNCIAS
DEPARTAMENTO DE FÍSICA

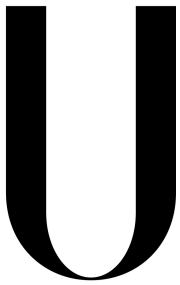

LISBOA

UNIVERSIDADE
DE LISBOA

Development of MRI radiofrequency coils to study neurophysiological changes in a neonatal animal model at 9.4T

Andreia Capaz Silva

Dissertação
Mestrado Integrado em Engenharia Biomédica e Biofísica
Perfil de Sinais e Imagens Médicas

2013

UNIVERSIDADE DE LISBOA
FACULDADE DE CIÊNCIAS
DEPARTAMENTO DE FÍSICA

Development of MRI radiofrequency coils to study neurophysiological changes in a neonatal animal model at 9.4T

Andreia Capaz Silva

Dissertação
Mestrado Integrado em Engenharia Biomédica e Biofísica
Perfil de Sinais e Imagens Médicas

Orientadores: Professor Doutor Alexandre Andrade
Professor Doutor David Thomas

2013

Resumo

A lesão cerebral hipóxico-isquémica é uma causa comum de lesão cerebral em recém-nascidos, resultando num alto risco de morte prematura ou deficiência. Estas lesões cerebrais devem-se a um fluxo insuficiente de sangue (isquémia) e a um fornecimento reduzido de oxigénio (hipóxia) ao cérebro, eventos que provocam lesões cerebrais agudas resultando numa série de acontecimentos que induzem lesão permanente e morte celular. O diagnóstico da lesão hipóxico-isquémica é difícil e uma detecção tardia da condição pode resultar num tratamento menos eficiente e posteriores sequelas neurológicas.

A introdução da ressonância magnética como ferramenta clínica para avaliação da lesão cerebral hipóxico-isquémica neonatal permitiu a determinação da localização, extensão e evolução das lesões cerebrais hipóxico-isquémicas, sendo a mais sensível e específica das técnicas de imagem. Diversas modalidades de ressonância magnética têm vindo a ser exploradas para avaliar lesões cerebrais hipóxico-isquémicas neonatais para avaliação de mudanças neurofisiologicas entre estas modalidades encontra-se a arterial spin labelling.

Arterial spin labelling (ASL) é uma técnica de ressonância magnética que mede a perfusão cerebral (fornecimento de sangue a um tecido capilar) de forma não invasiva. Nesta técnica o sangue arterial, que flui nas artérias que levam o sangue a uma zona que se pretende estudar a função, é utilizado como marcador endógeno. Utilizando um pulso de radiofrequência os protões das moléculas de água presentes no sangue arterial são marcados ficando o seu spin invertido. Através da subtracção de uma imagem da área em estudo com o spin arterial invertido e outra imagem com spin no estado não invertido é possível obter uma medição do fluxo cerebral. Para executar esta técnica uma bobina de ressonância de transmissão tem de ser utilizada para proceder à inversão dos spins, esta bobina pode ser a mesma com a qual se adquirem as imagens ou pode ser separada o que apresenta melhores resultados.

Outra técnica que tem sido explorada para fornecer informações metabólica em lesões cerebrais hipóxico-isquémicas é a ressonância magnética de sódio (^{23}Na). Esta técnica permite avaliar a viabilidade de um tecido, observando

as concentrações de ^{23}Na no tecido que se alteram quando um evento de hipóxico-isquémico ocorre. Apesar de ser uma técnica promissora as imagens de ressonância magnética de ^{23}Na apresentam menor relação sinal ruído e menor resolução. O desenvolvimento de novas técnicas de imagem beneficia dos avanços em várias áreas de ressonância magnética. A utilização de campos magnéticos mais elevados tem provado ser uma forma de melhorar as medições de quantificação, proporcionando uma maior sensibilidade e relação sinal ruído. Por outro lado a utilização de bobinas de radiofrequência especialmente desenvolvidas para cada técnica é também um meio utilizado para melhorar o desempenho de determinadas técnicas. As bobinas podem ser especialmente desenhadas para se adaptar a um determinado modelo em estudo ou para estarem de acordo com um determinado protocolo experimental.

O objectivo do trabalho descrito nesta dissertação é projectar e construir bobinas de radiofrequência (RF) que se destinam à utilização num sistema pré-clínico de ressonância magnética com um campo magnético de 9.4 Tesla. As bobinas desenvolvidas serão aplicadas em estudos de imagiologia neonatal utilizando um modelo animal (porco recém-nascido) com lesão hipóxico-isquemica. O principal foco do estudo principal em que o projecto descrito se insere é detectar as alterações neurofisiológicas decorrentes das hipóxico-isquemicas no cérebro utilizando diversas técnicas de ressonância magnética. Neste projecto em particular pretendem-se estudar duas dessas técnicas: arterial spin labelling e ressonância magnética de ^{23}Na.

O projecto foi dividido em dois objectivos principais. O primeiro objectivo consiste em projectar e construir uma bobina de RF de transmissão para ASL desenhada de acordo com as características do estudo experimental geral em que este projecto se insere. Pretende-se que a bobina seja posicionada na zona do pescoço do animal em estudo, o animal está deitado em pronação numa estrutura plástica cilíndrica desenhada para se encaixar numa bobina de volume que efectua a transmissão e recepção de radiofrequência que permite adquirir as imagens de protões. A bobina é posicionada entre o animal e a estrutura cilindrica.

O projecto foi desenvolvido para estar de acordo com os requisitos do procedimento acima descrito. Foi desenvolvida uma bobina de superfície sintonizada á frequência do hidrogénio a 9.4 Tesla (399.553MHz) e a impedância da bobina foi transformada de modo a corresponder á impedância dos cabos coaxiais e do sistema de ressonância magnética, neste caso 50Ω. A bobina apresenta um método de desassociação activa entre a bobina desenvolvida e a bobina de volume. Este método consiste na colocação de um díodo PIN em série com o circuito o que permite que a bobina seja sintonizada apenas quando é necessário a transmissão de RF. A bobina é conectada a um cabo coaxial, este cabo é um circuito não balanceado que interage com a bobina

levando a uma perda de sinal. Para diminuir estas possíveis perdas foram implementados dois tipo de circuitos, um junto à bobina e um circuito de um condensador em paralelo com um indutor implementado no cabo coaxial. Foi desenhada em 3D uma estrutura para proporcionar a protecção e acomodação da bobina. Para além disso foram construídos dois dispositivos que permitem a utilização da bobina. Um PIN diode driver que fornece a corrente necessária para a activação do díodo PIN e um Bias T um circuito que permite o fornecimento simultâneo de corrente continua e do pulso de radiofrequência à bobina. Todos os passos efectuados foram avaliados utilizando um analisador de redes, e os resultados foram apresentados sobre a forma de medições S11 ou S21 conforme o tipo de medição adequado.

O segundo objectivo consiste em projectar e construir uma bobina de transmissão e recepção de radiofrequência para imagens de ^{23}Na da região cerebral. Foi desenvolvida uma bobina de superfície sintonizada á frequência do ^{23}Na a 9.4 Tesla (105.683MHz) e a impedância da bobina foi transformada de modo a corresponder a 50 Ω. A bobina apresenta um método de sintonização remota à frequência desejada, o que permite que a sintonização da frequência e da impedância sejam realizadas fora da zona da bobina ou do magneto. A bobina apresenta um método de desassociação entre a bobina desenvolvida e a bobina de volume. Este método consiste na implementação de um circuito composto por um indutor e um condensador em paralelo com o circuito principal. Os resultados do processo descrito foram apresentados sobre a forma de medições S11 ou S21 conforme o tipo de medição adequado.

Para avaliar a bobina de transmissão e recepção para ^{23}Na foram adquiridas imagens de ressonância magnética de um fantoma e in vivo utilizando porcos recém-nascidos sujeitos a cirurgia para provocar a lesão hipóxico-isquémica. As imagens foram obtidas no sistema Varian 9.4T e os dados foram analisados usando Matlab. A bobina de superfície foi colocado dentro da bobina de volume de ^{1}H, a ser utilizado como referência para a localização da bobina e avaliação de informações anatómicas. As imagens in vivo foram adquiridas antes de ser efectuada a lesão hipoxica isquemica , 24 horas depois e 48 horas depois. Em ambos os caso foi possivel acquisição de imagens de ^{23}Na e detecção de diferentes estruturas.

Esta tese é composta por sete capítulos. O primeiro capítulo diz respeito à introdução da tese, no segundo capítulo apresenta-se uma introdução teórica ,na qual são descritos os conceitos subjacentes à teoria da técnica de ressonância magnética e ao desenvolvimento de bobinas de radiofrequência. É ainda complementada com uma breve descrição das técnicas ASL e ressonância magnética de sódio e resumo dos principais artigos publicados na área da ressonância magnética para estudo de lesões hipóxico-isquémicas neonatais.O terceiro capítulo descreve os materiais utilizados para o desen-

volvimento das bobinas de radiofrequência. Nos capítulos quatro e cinco é apresentado em detalhe o desenvolvimento das bobinas e resultados das avaliação das mesmas. O sexto capítulo apresenta as imagens de sódio, as imagens incluidas são resultado de experiências realizadas com fantomas e in vivo. No último capítulo são apresentadas as conclusões e futuros aperfeiçoamentos dos projectos.

Palavras-chave: Ressonância magnética (RM), Bobinas de RF, ASL, RM de ^{23}Na, 9.4 Tesla

Abstract

Advanced magnetic resonance imaging techniques have been used as clinical tools for assessment of neurophysiology changes. Arterial spin labelling (ASL) is a magnetic resonance technique that noninvasively measures brain perfusion. There are several labelling techniques, one such technique is to use an imaging coil and a separate labelling coil. Sodium MRI provides valuable metabolic information assessing tissue viability, it has much lower SNR and resolution than proton imaging however physiological information provided has already proved to be valuable.

In this project it is proposed to design and built a dedicated ASL coil and a transmit/receive sodium (^{23}Na) radiofrequency (RF) coil to provide images of an animal model (piglet) of hypoxic ischaemic (HI) injury at a 9.4T preclinical MRI scanner.

The proposed RF coils were designed and constructed. The process of development of each coil is described in detail: the tuning and matching process, the decoupling techniques chosen and the balancing methods applied. It is also presented the process of construction of other components required to allow the development or application of the coils in vivo.

The evaluation of both coils and other devices constructed is presented based on the adequate bench measurements. For the transmit/receive ^{23}Na radiofrequency coil the performance was also demonstrated performing MR imaging in a phantom and in vivo (piglet HI injury model). Sodium images of piglet's brain before HI injury, 24 and 48 hours after injury are presented.

Keywords: MRI; RF coils; ASL; ^{23}Na MRI; 9.4 Tesla

Acknowledgments

I would like to start my acknowledgements by thanking my supervisors.

I would like to show my immense gratitude to Dr.David Thomas for giving me the opportunity to work in this project, for his encouragement and for sharing his knowledge with me. I also wish to thank him for his patience and for being extremely supportive. I am extremely grateful to Dr.Aaron Oliver-Taylor, for his guidance and patience sharing his knowledge with me and for spending a huge amount of his time helping in my project. I thank his dedication to my project and his effort to teach me how to work better. I also would like to express my thanks to Professor Alexandre Andrade for always being available and helpful during my project and thesis writing and for the encouragement he provided me during the time I have been his student in the Faculty of Sciences.

A big thank you to Marilena and Patxi for their enthusiasm, for helping me in my project and cheering me up, you make the basement seem a sunny place. I also thank Dr. Mohamed Tachrount and Magda Sokolska for sharing with me their knowledge and for the help in the experiments. Many thanks to everyone in lab that helped me with the experiments or gave me support in some way.

Thank you to my friends, the ones I already knew and the ones I met during my journey in London. Your energy and friendship made my stay in London a unique experience which helped to be better in my work.

At last I would like to thank my family and friends for all their support and comprehension when I couldn't be present. I will always be grateful to my wonderful parents, Esmeralda and João José, and my sister, Ana Rita. I would like to thank you for always believing in me, even when sometimes I couldn't believe in myself. Without your love and encouragement this thesis, as well as everything else I achieved in my life, would not have been possible.

Contents

List of Figures

List of Abbreviations

ASL Arterial Spin Labelling.

CBF Cerebral Blood Flow.

DC Direct Current.

EMF Electromotive Force.

FOV Field of View.

GRE Gradient echo.

HI Hypoxic Ischeamia.

LC Inductor Capacitor.

MRI Magnetic Resonance Imaging.

MRS Magnetic Resonance Spectroscopy.

PCB Printed Circuit Board.

RF Radiofrequency.

SNR Signal to noise ratio.

TE Echo Time.

TR Repetition Time.

TSC Tissue Sodium Concentration.

TTL Transistor-Transistor logic.

Chapter 1

Introduction

Hypoxia ischaemia (HI) is a common cause of brain injury in newborn children affecting in between 1-10 per 1000 newborn children resulting in an high risk of early death and long-life disabilities [27]. HI is a combination of insufficient blood flow (ischaemia) and reduced oxygen supply (hypoxia) to the brain. These events may lead to acute brain injury and a cascade of events inducing delayed injury and cell death. Recognition of HI is difficult and a later diagnosis may result in less efficient treatment and subsequent neurological sequelae[40].

Neuromaging techniques such as cranial ultrasonography, computed tomography or near infrared spectroscopy have been used since 1960 to detect HI pathologies providing different information about HI [10]. Since the introduction of magnetic resonance imaging (MRI) as a clinical tool for assessment of neonatal HI brain injury major progresses have been done. MRI techniques allow determination of location, extension and evolution of HI lesions being the most sensitive and specific of the imaging techniques [5][10].In the last 20 years different modalities of MRI and magnetic resonance spectroscopy (MRS) have been used in clinical and experimental studies performed on animal models of HI injuries. One of the most suitable animals for neonatal HI brain imaging of metabolic and physiologic are newborn piglet, rodents are also used in follow up long-term outcomes[19].

Multiple MRI techniques have been applied to explore neonatal HI injury. Arterial spin labelling (ASL) is one example it measures brain perfusion (blood delivery to a capillary bed tissue) noninvasively. Cerebral blood flow is an indicator of cerebral metabolism and neuronal function [51]. In ASL arterial blood is magnetically labelled and then the distribution of the blood flow is imaged. To perform this technique an RF transmitter labels the arterial blood which can be done using the coil which performs images or using a separate RF transmit coil. Another technique that has been explored

to provide metabolic information in HI is ^{23}Na MRI. Sodium ions maintain cellular homeostasis, regulating important aspects of human body such as pH, osmosis or action potential in axons. In an hypoxic ischaemic event there are profound changes in the behaviour of the cells which will results in tissue sodium concentrations changes. ^{23}Na imaging provides valuable information about tissue viability[19].

The development of new techniques benefit from advances in several MRI areas. High magnetic field imaging has proved to be useful to improve quantification measurements, providing better sensitivity and signal-to-noise ratio. Each technique has unique hardware requirements and it is a great advantage to develop specific RF coils in house with the practical and RF requirements for a specific technique, specific animal model and experimental set up.

The project described in this thesis aims to study neurophysiological changes related to ASL and ^{23}Na MRI in neonatal models, the project is inserted in a research project that aims to study neurophysiology changes by application of several MRI techniques in an animal model (piglet) which closely mimics the clinical situation on a 9.4T preclinical scanner.

The work presented has two main goals: to design and built a transmit RF coil for ASL specially designed according the requirements of the main research project experimental set up and a transmit/receive RF coil for sodium brain imaging. It is part of the project goals to design the respective coil housing as well as hardware devices required to use the RF coils.

This thesis comprises a background chapter (chapter 2) presenting the theory underlying MRI theory and coil development. Chapter 3 consists of the instruments required to design and develop the RF coils. Circuit design, housing design, methods of development, implementation and results of ASL RF coil and ^{23}Na transmit coil are presented respectively in Chapter 4 and Chapter 5. Chapter 6 describes initial ^{23}Na imaging results, images presented were acquired for phantoms and in vivo. In Chapter 7 the conclusions of the project are discussed.

Chapter 2

Background

2.1 Magnetic Resonance Imaging

This subchapter briefly reviews the basics of MRI technique. The information is a compilation from references [28], [12], [21] and [38].

2.1.1 Nuclear magnetic resonance

Magnetic resonance imaging (MRI) is an imaging technique that produces images of biological tissue based on the nuclear magnetic resonance (NMR) phenomenon. The NMR phenomenon occurs when nuclei with non-zero spin interact with an external magnetic field B_0.

A nucleus is a combination of subatomic particles (protons and neutrons) each particle have a fundamental property the angular momentum also known as spin. A nucleus containing an unpaired number of subatomic particles is considered to have a rotating charge as a result of the spin which creates a magnetic moment. The simplest nucleus usually considered is the single proton, ^1H. However nuclei such as ^{13}C, ^{19}F ^{23}Na or ^{31}P can also provide NMR signal.

When a proton is placed in an external magnetic field B_0, the magnetic moment tends to align in the direction of the magnetic field experiencing a turning force known as torque. Due to laws of quantum mechanisms the magnetic moment do not fully align in the direction of the magnetic field, instead the magnetic moment precess around the magnetic field direction. In the presence of a magnetic field all protons precess at the same frequency that is proportional to the external field, given by the Larmor equation.

$$\omega_0 = \gamma B_0 \tag{2.1}$$

where γ is the gyromagnetic ratio, a constant dependent on the nucleus which is equal to 2.7×10^8rad s^{-1} T^{-1} for protons.

2.1.2 Equilibrium magnetization

In the presence of an external magnetic field spins will align either parallel (spin up) or anti-parallel (spin down) to the direction of the external magnetic field. The alignment orientation depends on the proton's energy, more energy is required in the anti-parallel direction than in the parallel direction.

The number of protons aligned in each state in equilibrium is different due to the energy required in each state. The ratio between states can be determined by a statistical distribution, the Boltzmann distribution and depends on the external magnetic field strength and on temperature. The difference creates a net magnetization M_0 given by

$$M_0 = \frac{\rho\gamma^2\hbar^2 B_0}{4kT} \tag{2.2}$$

where ρ is the proton density, k is the Boltzmann's constant and T is the temperature.

The magnetisation vector M_0 is a small vector parallel to the external magnetic field B_0 vector when in equilibrium. It has a small but measurable value which can lead to a measurable NMR effect when in certain conditions.

2.1.3 Excitation and Detection

In order to measure M_0 a radiofrequency (RF) pulse oscillating at Larmor frequency is generated producing a magnetic field B_1 perpendicular to B_0 . The B_1 field is produced by a transmitter coil.

The applied B_1 field rotates the magnetization vector M_0 out of the B_0 direction (z-plane) into a transverse direction (xy-plane), the new magnetisation vector is represented by M. Seen at a frame rotating at the Larmor frequency, M is a vector moving monotonically to the transverse plane. The application of a RF pulse also bring the spins to be in phase coherence. The angle between the magnetization vector and the main magnetic field is know as flip angle α and is given by

$$\alpha = \gamma B_1 t_p \tag{2.3}$$

where t_p is the pulse duration and B_1 is the magnetic field generated by the RF pulse.

The precession of the transverse magnetization around the main magnetic field creates a small magnetic field. This magnetic field is measured by a

receiver coil that detects the flux of the rotating magnetic field inducing an electromotive force (EMF) that is described by Faraday's law of induction. According Faraday's law of induction a time changing magnetic field will induce a EMF in a conducting coil perpendicular to that field.

The signal picked by the receiver coil is then processed by the MRI scanner.

2.1.4 Signal detection: Spatial localization

In the theory described above the magnetic resonance signal is presented as a global signal from a sample. In order to create MR images signal must be detected from different spatial locations in a process known as spatially encoding process.

In order to spatially encode the magnetization three different gradient fields in x, y and z direction are superimposed to the B_0 field.

There are three different encoding processes in order to acquire a 3D image. The slice-select gradient will allow the selection of specific slices of the sample to be imaged. Based on the slice selection a changing in the three orthogonal gradients will be applied encoding the signal as a function of frequency and phase.

The order by which of the encoding steps will occur depends on the image specificities required and different acquisitions protocols have been developed.

The collected data from each spatial frequency is stored in the k-space and applying a Fourier transform the signal is transformed into a MRI image.

2.1.5 Relaxation times

After the application of the RF pulse the spins, which were rotating in phase and in the transverse plan, will eventually restore the equilibrium state in a process known as relaxation.

The relaxation mechanisms depend on spins interction with the surroundings and behaves differently in different tissues. The relaxation of excited spins is based on two events: the re alignment of the net magnetization with the main magnetic field due to a loss of energy absorbed during the excitation and a dephasing of the spins which are in phase coherence when the rf pulse is applied.

Longitudinal Relaxation

Longitudinal relaxation or spin-lattice relaxation, refers to a phenomenon of energy transference from the spin system to the surrounding environment,

due to interaction of the spin system with external stimulating field coming from neighbouring protons and other nucleus.

These interactions cause the longitudinal component of the net magnetization vector to increase from M to M_0. The time that the longitudinal magnetization takes to return to the equilibrium position is a constant and is represented as T_1.

The longitudinal relaxation is described according to the following Bloch equation:

$$\frac{dM_z}{dt} = \frac{M_0 - M_z}{T_1} \tag{2.4}$$

Transverse Relaxation

Transverse relaxation or spin-spin relaxation refers to the phenomenon of loss of phase coherence of the spin system due to inhomogeneities in the B_0 field which lead to differences in the precession frequency of the spins.

The loss of phase coherence results in the disappearance of the transverse component of the net magnetization vector. In biological tissue, this process is significantly faster than longitudinal relaxation. The transverse relaxation has a time constant represented as T_2 and represents the time to lose the phase coherence. The transverse relaxation is described according to the following Block equation:

$$\frac{dM_x, y}{dt} = \frac{-M_{x,y}}{T_2} \tag{2.5}$$

Due to external field B_0 inhomogeneities there is a additional dephasing of the magnetization described by $T_2^{'}$.

T_2^* is the relaxation time that takes in to account both T_2 and $T_2^{'}$. This relaxation time is described by equation 2.6.

$$\frac{1}{T_2^*} = \frac{1}{T_2} + \frac{1}{T_2^{'}} \tag{2.6}$$

2.1.6 Pulse Sequences

Pulse sequences are series of gradients and RF pulses applied to generate MR images. Pulse sequences are presented as a scheme with several lines where there are instructions for the timing to the application of the RF pulse and each of the gradient fields. Each pulse sequence scheme will produce a different type of signal depending on the characteristics of the image required. when performing an imaging acquisition there are two main parameters to be

selected by the image operator, the time between the start of the RF pulse and the maximum in the signal this is called the echo time (TE). The other parameter is the repetition time (TR) of the sequence of pulses applied. New pulse sequences are being developed everyday however there are two main sequences from where all the others derive, the gradient echo (GRE) and spin echo (SE) sequences.

Spin echo

In SE sequences, a 90^o RF pulse is applied to flip the magnetization into the transverse plane. Due to the field inhomogeneities the spins start to dephase. In order to rephase the spins at one-half of the echo time a 180^o RF pulse is applied. At the echo time a echo is produced and read.

The signal equation from a general spin echo sequence is described as follows:

$$S = M_0(1 - e^{\frac{-TR}{T_1}})e^{\frac{-TE}{T_2}} \tag{2.7}$$

Gradient echo

In GRE sequences, an RF pulse is applied with variable flip angle , less than 90^o. Instead of the RF pulse the gradients are used to dephase and rephase the transverse magnetization. In gradient echo sequences the T_2 time takes in consideration the field inhomogeneities because the gradients do not refocus the field inhomogeneities, the value weighted is represented as T_2^*.

The signal equation from a general gradient-echo sequence is described as follows:

$$S = M_0 \frac{\sin\theta(1 - e^{\frac{-TR}{T_1}})}{1 - \cos\theta e^{\frac{-TR}{T_1}}} e^{\frac{-TE}{T_2^*}} \tag{2.8}$$

2.1.7 Ultra-High Field MRI

During the last decade MRI had a great development in many aspects of the MRI system. Many of the advances done in the MRI technique are related with the increase of the MRI field strength. The use of ultra-high field MRI scanners brought many advantages however with the advantages new challenges in equipment development were raised as well. MRI field is consider to be high when field strength is greater than 3.0 T and ultra-high when equal or greater than 7 T. For purpose of research studies have been conducted from low fields such as 1.5 T to 21.1 T[39].

The main reason for the use of ultra-high field MRI is the signal-to-noise ratio dependence on the strength of the magnetic field B_0. In theory at high fields the SNR is linearly proportional to the static magnetic field strength. The higher the magnetic field strength the better the image quality which improves the localization and quantification of either anatomic and physiologic properties. The high SNR can also allow a reduction in scanning time preserving image quality. Imaging nuclei other than hydrogen nucleus is improved with these ultra-high fields, since at lower fields SNR and sensitivity are low the introduction of higher field opened new avenues of research with other nuclei.

These higher fields strengths present challenges for hardware development as discussed in [38] and [46].

Due to susceptibility effects there are B_0 field inhomogeneities and wavelength length constraints lead to RF B_1 field inhomogeneities both B_0 and B_1 non-uniformities increase image artefacts.

At high RF frequencies there is less control in coupling between RF elements and the RF power requirements increase with the field which result in increased specific absorption rate. Other safety problems arise from the high frequency such as the coaxial cables behaving as antennas these problems can be mitigated and are discussed in subchapter 2.2.7 .

2.2 MRI Radiofrequency coils

This subchapter briefly describes the RF coils theory and design requirements. The information on this subchapter is a compilation from references [29], [46] and [28].

2.2.1 Electromagnetic theory

In a MRI system RF coils are used for the purpose of transmission and reception . A transmitter excites the magnetization vector while the receiver detects the signal that arises from the relaxation of magnetization and image encoding.

The electric and magnetic phenomenons related with these events are described by Maxwell equations.

The magnetic field created by electric current and a changing electric field is described according Ampere's law. The law states that in a closed loop path the line integral of the magnetic field intensity is equal to the sum of the current enclosed in the path and Maxwell's displacement current term. Ampere's law is described according to equation 2.9 [18]

$$\oint \overrightarrow{B} \cdot d\overrightarrow{s} = \mu_0 I_S + \mu_0 \varepsilon_0 \frac{\partial \Phi_E}{dt} \tag{2.9}$$

where μ_0 is the permeability of free space, ε_0 is the permittivity of the free space,Φ_E is the electric flux.

As previously described after excitation the rotating magnetic field creates an electric field due to the changing magnetic flux. According to Faraday's law, the electromotive force, a line integral of the electric field around a close path, equals the rate of change of a magnetic flux passing through the surface of the close path. Faraday's law of induction is described according to equation 2.10 [18]

$$\oint \overrightarrow{E} \cdot d\overrightarrow{s} = -\frac{d\Phi_B}{dt} \tag{2.10}$$

where Φ_B is the magnetic flux.

A transmitter coil must generate a uniform rotating magnetic field, that field must be rotating at the Larmor frequency of the nucleus to be imaged. While a receiver coil must have a high signal sensitivity at the Larmor frequency of the nucleus to imaged with low noise, maximizing the signal-to-noise ratio.

Signal transmission and reception may be performed using different coils: transmitter and receiver RF coils or a single coil can also be used for both transmission and reception.

According to the principle of reciprocity the sensitivity of a coil used as a receiver to detect the magnetization at a point is proportional to the efficiency of that coil when used as a transmitter, to generate a RF field at that same location[38]. In other words that means that a good transmitter is also a good receiver.

2.2.2 RLC Equivalent Circuit and Resonance

The main requirement to have a RF coil effective for imaging, is to build a circuit that is tuned to the frequency of interest, the Larmor frequency depending on the nucleus to be detected and the main magnetic field strength.

RF coils are described according to the principles of LCR circuits. In a LCR circuit there are an inductor (L) which in the case of the RF probe is the conductor, a capacitor (C) which is connected to the conductor in series or parallel and an electrical resistance (R). The LCR circuit is an oscillator forcing the current to oscillate at the resonance frequency required. A resonant circuit is achieved when at a certain frequency the imaginary components of the impedance of the coil cancel each other.

The Impedance (Z) of the coil has a real and an imaginary part and in the Cartesian form Z is given as:

$$Z = R + jX \tag{2.11}$$

where R is the resistance of the RF probe and X is the reactance.

The reactance is the sum of the capacitive and inductive reactances and is given as:

$$X = X_L + X_C \tag{2.12}$$

$$X_L = \omega L \tag{2.13}$$

$$X_C = -\frac{1}{\omega C} \tag{2.14}$$

where ω is the angular resonant frequency and is measured in rad^{-1}.

When the coil is resonating the reactance is zero and the resonant frequency (f_0) in a LC circuit is expressed by:

$$f_0 = \frac{1}{2\pi\sqrt{LC}} \tag{2.15}$$

where the resonant frequency is measured in Hz or s^{-1}.

At the resonant frequency the reactances terms cancel each other and the impedance of the circuit is a purely resistive value. The energy in the circuit oscillates it can be stored as magnetic energy in the conductor's inductance or as electric energy in the capacitor.

In a RLC circuit the inductor and the capacitor can be placed in parallel or series configuration.

(a) Series LC circuit **(b)** Parallel LC circuit

Figure 2.1: LC circuits configuration

In series configuration, represented in figure 2.1a, at resonance the current flowing in the circuit is maximum and the impedance is zero if the components are ideal components. However real components have some associated

resistance which does not allow the impedance to reach zero . In parallel configuration, represented in figure 2.1b, at resonance the current flow is blocked due to a theoretical infinite impedance which is reduced to a finite value in real circuits.

Losses

When the RF coil is at resonance the reactance parts of the components are cancelled and there is an energy dissipation through the resistance generated in the circuit. This resistance arise from several loss sources.

The sources of loss can be divided in two main categories, the resistive losses and radiative losses. The resistive losses also designated ohmic losses are the sum of the real resistances of the components of the coil such as the type of conductor component and the surface area, the capacitors, the solder or the pin diodes. A careful choice of these components as well as a well designed and produced coil may reduce this type of losses.

In radiation losses, there is a radiative field that loses energy to the coil environment (the subject, the magnet conductors and free space).These type of losses depends on the design of the coil and the type of environment and it increases with an increasing field strength. The radiative losses are described as the difference between the input power to the coil and the ohmic losses.

Distributed capacitance

As previously described to tune a RLC circuit to the resonant frequency the inductor or the capacitor may be varied. In RF coil design the easiest procedure is to use a conductor with an intrinsic inductance given by the shape of the coil and tune the coil using a variable capacitor. In general, to reduce radiative and dielectric losses in the RF coil design there are several capacitors distributed. Capacitors are distributed in series in the coil, as described in equation 2.16:

$$\frac{1}{C_{T_{total}}} = \Sigma \frac{1}{C_t} \tag{2.16}$$

Although distributed capacitance will minimise losses there are disadvantages if many capacitors are placed in the coil. In order to maximize the benefits of the method a compromise has to be done between the number of capacitors and the resistance of the coil that may arise because of the equivalent series resistance that is present in capacitors and soldered connections.

2.2.3 Quality factor and Signal-to-Noise Ratio

A coil is characterized by the ability to store energy versus the energy that is dissipated by the coil. This ratio describes the efficiency of a coil and is known as the quality factor or Q factor.

In a RLC circuit is given as

$$Q = \frac{\omega L}{R} \tag{2.17}$$

where R is the resistance of the component.

Q factor can also be calculated as a ratio between the center frequency and the difference of frequency existing at the half peak power, it is calculated as:

$$Q = \frac{f_0}{\triangle f} \tag{2.18}$$

In a well constructed coil, if the coil is not loaded it must have a high Q value, and when a conducting sample is placed near the coil the Q value is expected to decrease.

The quality of the RF coil influences the quality of the final acquired image. The signal-to-noise ratio is a parameter used to determine the quality of any image. A design goal in a RF coil is to maximize the image SNR. SNR is the ratio between the amount of signal detected, based on the tipped magnetization and the strength of the magnetic field, to the amount of noise based on the thermodynamic principles.

2.2.4 Matching

To transmit the signal detected by the RF coil, the coil is connected to a pre-amplifier through a transmission line, usually a coaxial cable. A transmission line has a characteristic impedance, in order to have an efficient power transfer it is crucial to match the impedance of the coil and the coaxial cable. Typically 50Ω is the impedance value to which the components match. An unmatched circuit results in a reflection of the signal that is supposed to be transmitted or receipted by the coil. Resulting in a decreased delivered RF power of the transmitter and a loss in signal in the receiver. The reflection coefficient Γ is defined as:

$$\Gamma = \frac{Z_{coil} - Z_{TL}}{Z_{coil} + Z_{TL}} \tag{2.19}$$

where Z_{TL} is the transmission line impedance.

When $\Gamma = 0$, all the power is transmitted and reflections are eliminated. In conclusion when $Z_{coil} = Z_{TL}$ a maximum signal is transferred.

The initial impedance of coil is usually different from the cable impedance, to match coil impedance many matching networks can be implemented. A simple technique to match a coil consists of adding a capacitor in parallel to a LCR parallel circuit, changing the resonant peak to the match impedance usually 50Ω.

2.2.5 Decoupling

When multiple coils are placed near each other they interact. From Faraday's induction law the EMF of one coil induces current in the other. During transmission the receive coil disturb the homogeneity of magnetic fields and artefacts may arise, the strong B_1 field can also induce RF currents in the receive coil damaging the system and more power will be required to achieve a certain flip angle. During reception the SNR of the receive coil decreases.

Coupling may arise from coils resonating at the same resonant frequency or with two coils of different resonant frequencies. To prevent coupling different techniques are available.

To decouple coils resonating at the same resonant frequency the coils are detuned. To avoid the coupling effect it is necessary to detune the coil that it is not in use. Detuning circuit is performed in passive or active configurations. In both configurations the detuning is achieved using PIN diodes.

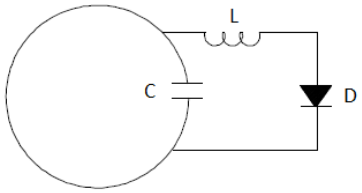

Figure 2.2: Parallel active detuning[8]

In active detuning the diode can be place in parallel or in series with the coil circuit. In the parallel configuration (figure 2.2) when the PIN diode is forward biased (by applying a DC current) the capacitor C and the inductor start to resonate generating a large impedance that does not allow the current to flow in the RF loop [8].

In the series configuration the PIN diode is placed in series with the resonant circuit. The RF coil can be permanently switched off and to operate

the PIN diode must be forward biased [8].

Two coils resonating at different resonant frequencies placed near each other can be decoupled by placing a trap circuit in the lower-frequency coil.

A trap circuit consists of an inductor and a capacitor in parallel resonating at the higher frequency placed in series in the lower frequency coil to block the higher frequency of the two coils involved. In this methodology the coil where the trap is placed behaves as an open circuit at the higher frequency. This trap configuration blocks current at the higher frequency but allows RF current at the lower frequency [9].

2.2.6 Common mode effects

A coil that is tuned and matched is ideally a balanced circuit, at coil's terminals current flows symmetrically equal establishing a differential mode signal, a differential mode current. However the coaxial cable that connects to the coil is an unbalanced circuit. The coaxial cable generates common mode currents due to currents that passes through the shield these currents interact with the electromagnetic field generated by the coil.

These effects generate additional loss and if contact is made with the cable there is a risk of burning. At higher field strengths the signal wavelength can approach the coaxial cable length , which can make the cable behaves as an antenna. The coaxial cable can also couple with other conductive circuits adding additional losses.

Balance

To ensure correct operation of the coil and the safety of the subjects, common mode currents must be minimized using a balun (balanced to unbalanced) device. These are devices that can convert balanced to unbalanced currents and vice-versa. A balun can assume different forms and be located in different parts of the system. The first approach to reduce common mode currents is to create a symmetry in the coil circuit. To achieve this symmetry a lattice balun can be designed, the lattice balun consists of two capacitors with the same value and two inductors crossing the capacitors resonating at the resonant frequency of the coil.

The remaining approaches consist on blocking the current that flows on the coaxial cable shield. To block the current a parallel LC circuit is placed in series with the coaxial cable. This parallel circuit can be placed around the coaxial cable or connected in between two parts of the cable.

2.2.7 RF coils

In the process of construction of a coil several requirements should be taken in to account. A coil can be a transmitter or a receiver or both and the designs of construction are multiple. The type of design will depend on many factors such as the type of study, the region of interest to be imaged, the need for high uniformity of the transmitted field, a high SNR and other criteria. RF coils are usually customized products that will serve the specific needs of the user. In terms of general design RF coils are divided in two main categories: volume and surface coils.

Surface coils

Surface coils design are based on a loop shape, for example a rectangular or circular shape. They are placed near the region of interest. This type of coils produce images with a high SNR close to the coil due to the limited size but the field of view and penetration depth are reduced. The homogeneity of the image is also compromised. In order to extend the field of view it is possible to combine surface coil into arrays. When placing a surface coil care must be taken on the position of the coil in order to ensure it is perpendicular to the main magnetic field.

Volume coils

A volume coil is placed far from the surface and is used to cover a large volume of a sample allowing homogeneous transmit and receive sensitivity. The signal of this type of coil can be driven in quadrature. The volume coils assume many types of designs according to the their function. The main known designs are the birdcage coil and the TEM coil. Usually in clinical systems there is a large volume coil that transmits the signal and a surface coil for reception.

2.3 Arterial spin labelling to assess neonatal HI

Arterial spin labelling (ASL) is a magnetic resonance technique that can measure noninvasively brain perfusion (blood delivery to a capillary bed tissue) in particular cerebral blood flow (CBF). CBF measurement is an indicator of cerebral metabolism and neuronal function allowing assess to information about tissue viability and function [51].

In ASL magnetically labelled arterial water is the endogenous tracer used to measure perfusion. An RF pulse is applied to label an arterial region

changing the magnetization of the arterial water (by inversion or saturation) and subsequently an image is acquired at the area where it is expected to observe the blood flow. The water magnetization is different from the static tissue magnetization. A control image is also acquired where arterial water and static tissue have the same magnetization. The labelled image is acquired after a specific time in order to the labelled blood achieve the capillaries where blood exchange with tissue. In a particular voxel the difference between both images reflects the local perfusion in that voxel. Based on this difference a cerebral blood flow map is then computed. In order to ensure sufficient SNR multiple images are acquired [4]. The quantification of CBF is based on tracer kinetics theory first presented by Kety and Schmidt that was then adapted to ASL measurements. In this model applied to ASL the free diffusible tracer is the labelled arterial water. Using modified Bloch equation that include the blood flow effects in brain the model describe the brain tissue magnetization

There are two main types of ASL based on label sequences: continuous ASL (CASL) the arterial water is continuously labelled and pulsed ASL (PASL) where a thick slab of arterial water is labelled and images are acquired after a time that allows exchange blood and tissue. Other sequences such as pseudo CASL (pCASL) or velocity selective ASL (VSASL) were developed to overcome the limitations of the main sequences.

The following text will focus on CASL since it is the sequence which is intended to be used in the project.

2.3.1 CASL

In CASL, the arterial water labelling occurs by inversion of spins using a technique known as flow-driven adiabatic fast passage. This type of magnetization is achieved applying a continuous RF pulse, a long pulse with duration of $2 - 4s$ and at the same time applying in flow direction a magnetic field gradient.

Adiabatic inversion is achieved if the labelling process happens faster than T1 and T2 relaxation times and if the effective magnetic field orientation changes at rate that allows a constant angle between the effective magnetic field and the net magnetization [4].

Due to long off resonance RF pulses applied to label there is a decrease in signal due to the magnetization transfer (MT) effects. MT effect is present in the labelled image and not present in the control image. The subtraction will be showing both CBF and MT effects because images will have different magnitudes of saturation in tissue.

There are many ways to suppress such effect. It is possible to apply an off resonance pulse to the control image in order to create a MT effect similar to

the one generated to the labelled image. It is also possible to circumvent the problem using separate coils to label and image. One is placed on the neck to label blood the other is placed on the head in order to acquire images. This approach completely suppresses the MT effects moreover it is possible to select the carotids to label which allow selective measurements.

However such technique requires hardware that is not usually available on clinical scanners, such as separate transmit channel and detunable RF coil, other constraint of CASL is the need for special RF amplifiers that allow continuous excitation. Another disadvantage is that label region is far from the imaging slice which can decrease the magnetization signal due to relaxation times. CASL is still the most advantageous technique when there is a need for a high SNR [36].

2.4 Sodium imaging to assess neonatal HI

Since the 80s that sodium MRI has been considered useful to detect ischemia [15][30]. Sodium MRI can provide valuable metabolic information. In particular allows assess to tissue viability by observing changes in tissue sodium concentration (TSC) [19]. In an ischaemic event there is a deficient delivery of oxygen to the cells which cause damage ultimately leading to an increase in TSC [3].

Sodium nucleus (^{23}Na) has gyromagnetic ratio of $\gamma = 11,262 MHz \setminus T$ and nuclear spin of $3 \setminus 2$. In vivo sodium concentration is approximately 140 mM outside the cell and 10 mM inside the cell [7]. In comparison with ^{1}H, ^{23}Na nucleus has lower gyromagnetic ratio and low tissue concentration being 2×10^{-4} of ^{1}H concentration which means that signal-to-noise ratio is also lower in ^{23}Na imaging.

Due to the spin of $3 \setminus 2$ ^{23}Na nucleus has relaxation times T1 and T2 shorter than ^{1}H leading also to constraints in ^{23}Na imaging. Under in vivo conditions T1 value is between 30 and 50ms and in order to compensate the loss in SNR short repetition times are required. In vivo transverse magnetization has a biexponential decay, two T2 times are observed a slow component of 20 ms and a fast component of 2 ms. Most biological tissues are dominated by the fast T2 component requiring short echo times in between 0.2 to 0.4 to reduce T2 losses [43][35].

Due to ^{23}Na nucleus properties in vivo sodium imaging may deal with technical issues however it is possible to improve MR sensitivity in sodium imaging. Sensitivity can be improved increasing magnetic fields leading to an increased resolution while allowing smaller acquisition times [39].

^{23}Na imaging also requires new designs of RF coils, it is useful to include proton imaging capabilities to assess anatomical information along with the physiological data provided by sodium imaging. Many approaches have been described to allow both images. Two single tuned as well as double tuned coils have been studied as well as the use of surface and volume coils depending on imaging requirements and facilities available [52].

Although it is possible to acquire sodium images using standard acquisition schemes they are not the most suitable in ^{23}Na MR imaging which leads to other area of improvement. It is necessary to design pulse sequences that can provide short TE. During the last years many approaches have been described [1][41]. However it is still possible to acquire images with an acceptable SNR and resolution using GRE sequences allowing sodium imaging without use of demanding reconstruction methods and different gradient hardware [7].

Sodium imaging has much lower SNR and resolution than proton imaging however physiological information obtained by sodium MRI imaging has proved to provide important information in a great variety of diseases where TSC changes play an important role. It is a potential diagnostic tool in clinical environment and enables to follow the progression of diseases in research environment.

2.5 State-of-art of MRI techniques to assess neonatal HI injury

More than two decades ago, Nalin at. al (1989) reported the advantages of MRI to assess information of neonate with hypoxic ischaemic encephalopathy. In the article references to other articles stated that MRI and MRS were already showing valuable information. Information from morphological and functional aspects of cerebral perfusion using intravoxel incoherent motion were reported as well as metabolic information from phosphorus(^{31}P) and proton (^{1}H) MRS. Based on previous studies such as [23], Nalin at. al discuss the different types of lesions and conditions identified at the time with conventional T1 and T2 weighted MR imaging [32].

Martin and Barkovich(1995) described MRI findings based on several studies of term and preterm neonates, showing different patterns of T1 and T2 weighted images based on the timing of imaging after injury and if the MRI was conducted in a term or preterm neonate. The main conclusion was that MRI signal was difficult to detect in the first days of life [26].

Barkovich at. al (2005) applied conventional MR imaging, diffusion tensor imaging (DTI) and ^{1}H MRS to study changes in early patterns within 2

weeks in 10 neonates. Study conclusions were that both extent and pattern of injury change during time. In proton spectroscopy and DTI , patterns of HI can be detected at earlier times [2].

Chau et. al suggested that a predominant pattern of injuries are consistent on two weeks MRI follow-up. Following this study Chau stated in a different paper that is safe to consider diffusion-weighted imaging a valuable imaging technique in HI injury diagnostic [6]. This conclusion is extensively proved in other papers using apparent diffusion coefficient(ADC)and fractional anisotropy [42][47][24].

Perfusion can play an important role in HI injury detection. There are several techniques to assess tissue perfusion, using contrast enhancement or applying arterial spin labelling which does not require contrast administration and allow quantification of cerebral blood perfusion. Although there are studies [50][11] suggesting the possibilities of ASL in neonatal HI injury, there are just few studies focusing on ASL perfusion imaging in neonates with HI injury.

In Wintermark at. al (2011) study MR conventional imaging and ASL was performed to assess brain perfusion in 18 asphyxiated neonates. In the study ASL perfusion imaging allowed identification of neonates at risk to develop brain injury. Data collected suggests that neonates at risk had initial hypoperfusion flow and then hyperperfusion flow in specific brain areas. Findings were similar in neonates treated with hypothermia. The study also conclude that hypothermia does not prevent HI injury in early hyperperfusion. The study presents a limitation, accuracy of results is limited because labelling is found mainly in the major arteries and the entire label may not reach the imaging plane. Wintermark and colleagues proved the feasibility of the ASL method in neonatal HI injury [54].

Piennar and colleagues (2012) presented a method to compare apparent diffusion coefficient assessed by diffusion weighted imaging (DWI) and cerebral blood perfusion assessed by ASL (pseudo-continuous sequence) in neonates with HI injury. 9 neonates with evidence of ischaemia and 6 without evidence of MRI abnormalities underwent MR imaging (1.5T scanner). Piennar and colleagues conclude that there is a correlation between decreased ADC values and increased ASL cerebral blood perfusion values. The study suggests that hyperperfusion and ischaemia are associated [37].

MR spectroscopy such as ^{1}H and ^{31}P has been applied to assess an earlier diagnostic of HI injury measuring concentration of metabolites in specific brain areas. In proton spectroscopy many metabolites can be assessed,such as the ratio of lactate over N-acetylaspartate (NAA), usually observations of a decrease in NAA and increase in lactate predict HI injury timing. ^{31}P MR spectroscopy detects changes in the cerebral energy metabolism, measuring

the phosphorylated metabolites [25].

In piglet models of hypoxia ^{31}P spectroscopy measure levels of triphosphate and phosphocreatine to follow the duration of an hypoxic event [45][48].

Vial at. al (2004) proved the utility of MRI imaging and MRS to study neuropathology as a result of two acute cerebral HI induced to newborn piglet model and damage monitorization for 7 days. MRI and MRS studies performed in a 2.35-Tesla Bruker scanner with a double-tuned Helmholtz coil ($^1H/^{31}P$).^{31}P and ^1H MRS offers the ability to monitor the severity of the HI insults by monitoring cerebral phosphorylated metabolites and Lactate (Lac) respectively and T2-weighted images made possible to monitor the evolution of ischaemic lesions [48].

Thornton at. al and Munkebye at.al also published studies using piglet model to assess MRI and MRS information [45][31]. Lodygensky review describe other animal models papers that study changes in MRI in HI neonatal injury.

Sodium imaging is not found in literature to study neonatal HI injury however measure tissue sodium concentration can be useful to assess information of viability of tissue after HI injury. In LaVerde et. al and Atkinson et. al papers tissue sodium concentration has increased levels after an ischaemic event [22][1].

Chapter 3

Tools and Materials

3.1 Target Hardware

The RF coils developed were designed to be integrated into the standard imaging protocol used in a study of neonatal piglet model currently in progress at the Institute of Neurology, UCL. The imaging protocol is performed in a 9.4T Agilent MRI pre-clinical scanner for small and medium size animal.

Coils design is physically constraint to the dimensions of a transmit/receive proton volume coil (two channels) with a inner diameter of 150 mm (Figure 3.1a) and ultimately to a pod specifically designed to fit in the volume coil and to accommodate the subject being studied (Figure 3.1b).

The tuning frequency of each coil is dependent on the operating frequency of this specific scanner and matching impedance required is 50 Ω.

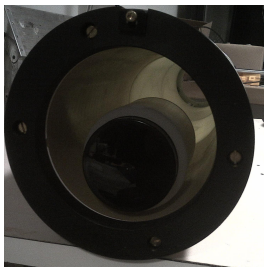

(a) Volume coil

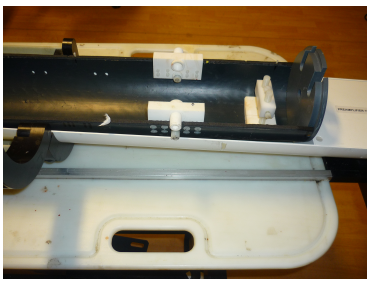

(b) Pod to accommodate the subject

Figure 3.1: Hardware setup

3.2 Network Analyser

The construction of the RF coil is tested using a vector network analyser. This is a test system that enables the characterization of performance of

radiofrequency devices. Generally it transmits a signal to the device to be tested and measures the response of that device. A network analyser measure wave reflection and transmission. Typically a network analyser have two ports, where a reflected wave can be measured in the same port of the incident wave and a transmitted wave can be measured with the a second port. Measurements are performed using scattering parameters, which measure not total current or voltages, instead it is measured the relationship between the incident and reflected or transmitted wave.

S parameters

At high frequencies measurements of total voltage or currents are hard to perform. S parameters perform voltage travelling waves measurements which are easier to acquire, these type of measurement do not require loads on the device to be tested. S parameters are related to measurements such as gain, loss, and reflection coefficient.

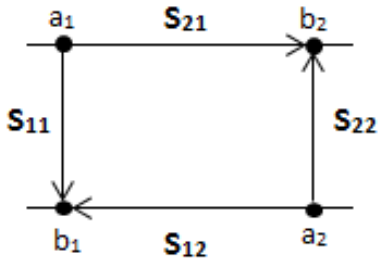

Figure 3.2: S-parameters

The scheme presented in Figure 3.2 represent the relationship between the voltage travelling waves - incident terms (a_1, a_2) and the output terms (b_1,b_2) - and the S parameters. The network analyser have four S parameters: S11- forward reflection coefficient, S12-reverse transmission coefficient, S22-reverse reflection coefficient, S21-forward transmission coefficient. Where the first number is the port where energy is measured and the second port where the stimulus is applied. In a S11 measurement RF stimulus is applied at port one and the reflected power is measured at port 1. In a S21 measurement an RF stimulus is applied at port 1 and power emerge at port 2. Depending on the measurement S-parameters can be displayed in different formats such as linear scales, logarithmic scales or smith charts. [44]

When building and testing MRI coils usually only the S11 reflection and S21 transmission coefficients are used. Typically the S-parameters are dis-

played on a logarithmic scale (decibels) versus the frequency.

Equipments used in this thesis to perform bench measurements were: an Agilent N9912A FieldFox RF Analyser (Agilent, Inc. Santa Clara, CA, USA)and an HP 8712C Vector Network Analyser (Agilent Inc., Santa Clara, CA, USA).

(a) Agilent N9912A FieldFox RF Analyser

(b) HP 8712C Vector Network Analyser

Figure 3.3: Network analysers

Agilent N9912A FieldFox RF Analyser is a portable device, which is useful to perform measurements inside of the magnet room. It is also easy to transfer data from the device to a computer. However the FieldFox RF Analyser do not perform Q measurements, this information was accessed using HP 8712C Vector Network Analyser.

3.3 Design Tools

Several software tools were used in the different stages of the project. An electronic simulation of the devices was performed using QUCS-Quite Universal Circuit Simulator (`http://qucs.sourceforge.net`) and Circuit Lab (`https://www.circuitlab.com`). Printed circuit board (PCB) layout was designed using KiCad (`http://www.kicad-pcb.org/display/KICAD/KiCad+EDA+Software+Suite`). PCB milling design was performed using VCarve Pro (`http://www.vectric.com/products/vcp/features.htm`). 3D objects were design on Autodesk Inventor Professional 2013 (`http://www.autodesk.com/products/autodesk-inventor-family/overview`) software. Image analysis was performed with custom programs developed in MATLAB from the MathWorks (`http://www.mathworks.com/products/matlab/`).

Required PCBs are designed with VCarve software and are then milled with a Marchant Dice LTD. CNC milling machine recently installed in the RF laboratory at the Institute of Neurology.

3D printed objects were printed at The Bartlett School of Architecture where 3D printing facilities are available to students use.

3.4 Bench test equipment

To test RF coils and other RF components it was also necessary to use devices specially designed to specific situations.

Shielded Loop Probes

A single shielded loop, as represented in Figure 3.5d, is used to detect or induce a magnetic field [17]. When two single shielded loops are placed together as shown in Figure 3.5b and 3.5c they can be used to evaluate resonant circuits, the double loop behaves as a transmit and receive system. The resonant circuit will couple with the loop transmitting at the resonant circuit and the second loop receives [34].

Two single loops were built using semi-rigid coaxial cable, and connecting at the end of the loop the inner conductor to the cable shield and soldered together, with loops with radius that can achieve 105 MHz frequency resulting in the probe shown in Figure 3.5c.

Since it is a transmit/receive device it must be connected to the network analyser in the S21 mode and the nulling of the probe can be adjust moving the loops. The overlap of the loops can change in order to null the probe at the desired resonant frequency. In Figure 3.4 the S21 measurement is presented which shows the nulling of the shielded probe achieved at frequency 105 MHz. The shield double loop shown in Figure 3.5b has smaller radius and achieve higher resonant frequencies.

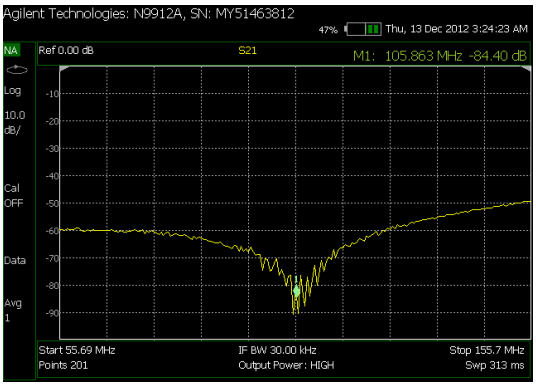

Figure 3.4: Probe Null at 105 MHz

The following devices previously were already constructed and are de-

scribed in [34].

These are devices usually used to test different types of RF devices. **Current probes** (Figure 3.5e) are done using a loop of semi-rigid coaxial cable around a ferrite ring. A magnetic field is generated in the system due to electricity flowing in the coaxial cable this type of probe is used to measure common mode shield currents.

A **monopole antenna** (Figure 3.5f) irradiates energy, producing and detecting electric fields. This type of antenna can be built with coaxial cable exposing a part of the inner conductor.

An **aluminium bed** (Figure 3.6) was used in measurements to produce a good conductive ground plane. On the the extremities of aluminium bed wood blocks are attached in order to fix cables and devices being tested.

Apart from these devices **ferrite rings** (Figure 3.5a) were also used during the bench tests. These are magnetic components used in RF components tests out of the scanner room. These ferrite rings, have different designs they can be clamped around cables or cables can be wrapped around the ring. Ferrite rings are used to absorb energy reducing cable currents.

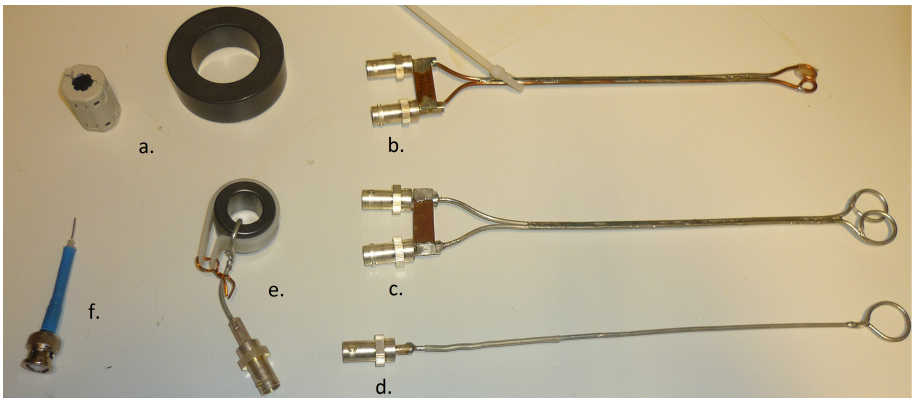

Figure 3.5: Probes: (a) Ferrite rings (b) Shielded Double Loop Probe (High Frequency) (c) Shielded Double Loop Probe (Low Frequency) (d) Shielded single loop probe (e) Current probe (f) Monopole antenna

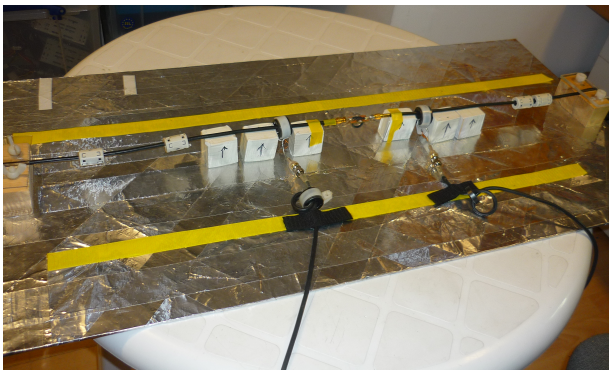

Figure 3.6: Aluminium bed

3.5 Phantoms

Different phantoms were developed in order to be used in the different stages of the project. A first phantom was construct to perform bench measurements and then other phantoms with different characteristics were constructed to perform imaging tests.

3.5.1 Testing phantom

A saline phantom was developed to be used in tuning and matching measurements. The main goal of the phantom is to have the same loading conditions that the piglet brain head has inside the volume coil presented in section 3.1.

A piglet was placed inside of the volume coil as usually done during the imaging protocol. The two channels of the volume coil were tuned and matched to the proton frequency at 9.4T and $S11$ measurements were saved using the Network analyser.

A plastic cylinder bottle was used as a container for the phantom in the bench measurements the bottle was 90 mm in diameter, 170 mm in length, and 1000 mL in volume. The bottle was filled with distilled water and then was placed inside the volume coil. The $S11$ trace was observed in order to understand the loading performed by the volume of the bottle on the volume coil. After that NaCl was added to the bottle in intervals of 0.1 gram until the $S11$ traces matches the saved traces of the piglet load. The final solution that filled the phantom was consisted of 3.6 g NaCl in 1000 ml H_20 (distilled water), phantom is shown in Figure 3.7.

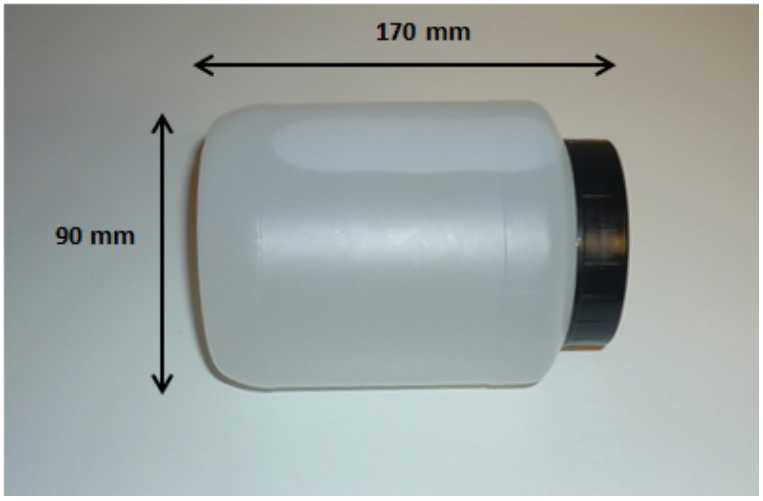

Figure 3.7: Test phantom

Chapter 4

ASL labelling system

As stated in the introduction section, the overall aim of the project is to study neurophysiology changes by application of advanced MRI techniques in an animal model, a newborn piglet suffering brain HI injury.

As described in section 2.3 to perform CASL imaging it is required a mean of excitation to label the blood in a part of the body and a mean of transmission and reception to perform imaging.

In this project a separate transmit RF coil is developed to perform excitation, the coil is specifically designed to the animal model under study and to the requirements of the target hardware described in section 3.1.

The following chapter describes the experimental procedure followed to develop a transmit surface coil and other hardware that allows the use of the ASL labelling coil in a MRI scanner such as a pin diode driver and bias tee.

4.1 ASL labelling coil: Methods

The ASL labelling coil was designed to be placed on the neck surface of the newborn piglets, where the carotid arteries the target structures for labelling are placed. According to measurements done in newborn piglets under experiment and from literature data it is known that carotid arteries are separated in less than 3 cm. For that reason it was decided that a small single surface coil is enough to label left and right carotid arteries.

The piglet is placed in the pod shown in figure 3.1b, in prone position, in order to allow good RF transmission the coil is placed in between the pod and the piglet. The piglet under experiment goes under surgery before, after surgery the piglet has a breathing tube placed in the neck, due to that reason many fluids will be present in the pod. In terms of housing the conditions require that the coil is completely sealed to avoid any contact between coil and fluids.

As it was previously said a volume coil is used as imaging element. The labelling coil must be actively decoupled from the volume coil to avoid RF deposition.

Coil developing process is described by steps, first a circuit design and coil housing design are presented. Following that the tuning and matching process, detuning, and coil balun set up is described in detail. At last cable trap methods of construction are also described.

4.1.1 Design

4.1.1.1 Circuit Design

The circuit design for the RF transmit coil is constructed according to figure 4.1. The circuit consists of a circuit with 4 capacitors ($C_1 - C_4$) distributed in a rectangular path circuit. A PIN diode (D) is placed in the circuit for active detuning and a RF choke (L_3) is connected between ground and the anode of the diode to allow DC bias supply. A lattice balun consisting of two capacitors (C_5, C_6) and two inductors (L_1, L_2) are present. A cable trap consisting of a capacitor (C_7) and an inductor (L_4) is attached to the circuit.

Details on the chosen methods and construction of each part of the coil is described in the following sections.

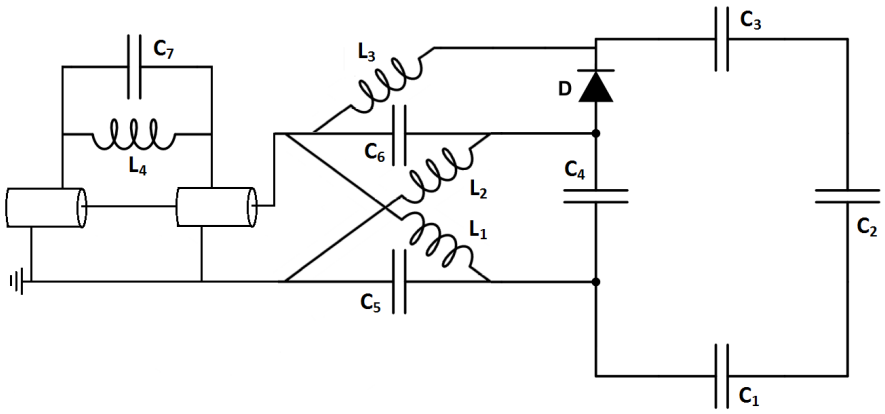

Figure 4.1: ASL labelling coil circuit

4.1.1.2 Practical Design

Coil shape and dimensions were chosen according to carotids position and to produce a B_1^+ field which has penetration depth that allows carotid labelling.

The final coil board was designed on VCarve Pro software, the software allows detailed design of the coil and milling specifications.

The coil has a rectangular shape with rounded edges as shown in Figure 4.2, with inner dimensions (40mm - 20mm) and outer dimensions of (55.20mm - 54.20mm). The corners are rounded in order to create uniform current flow, since sharp corners might create non-uniformities.

The transmit surface coil was constructed using copper clad FR-4 laminate which is a circuit board layered with copper on one side of the board. The circuit was printed using a milling machine. The created loop has a track width of 5.6mm, this track width permits placement of two capacitors in parallel in each capacitor gap. The capacitors used in the coil are ATC series B and according to datasheet, capacitors dimensions are: 2.79 x 2.79 x 2.54mm . Due to capacitors length the four gaps have 2mm of length. The PIN diode gap placed between two capacitors gaps is 1 mm length.

Two tracks are milled separated from the coil principal track in order to permit the isolation of the coil which is necessary to perform coil measurements. A second gap in both tracks is present to perform balun implementation and connection to coaxial cable.

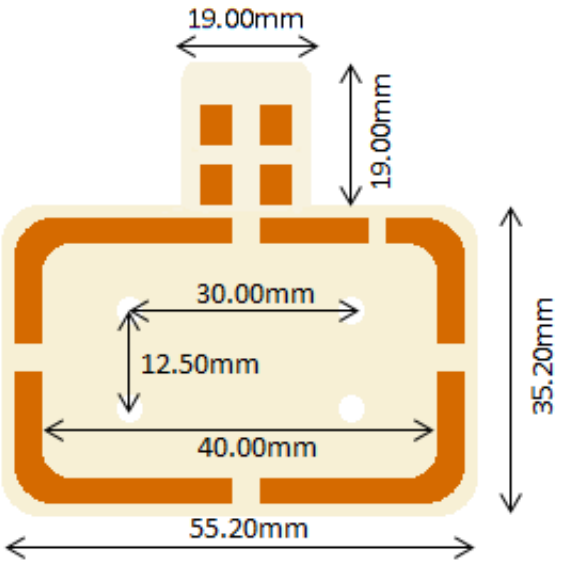

Figure 4.2: PCB design

4.1.1.3 Housing Design

Housing coil has an important role on the behaviour of any coil, preventing physical damage of the coil and preventing the excess of loading. This is even more relevant when the coil is to be surrounded by liquids that can damage

the coil. This coil is placed between a cylindrical pod and the neck of the piglet which has a breathing tube.

Autodesk Inventor software was used to design the housing features as shown in figure 4.3.

To meet the above requirements, two parts were designed a lid, a grey piece on the top in figure 4.3 and a box grey piece under the lid in figure 4.3. The blue piece represents coil PCB.

The **lid** is designed so that the outside feature is curved matching the cylinder pod.

The **box** is attached to the coil using nylon screws in order to have the coil placed near subject's neck. On the box part a hole is drilled to allow placement of a gland and grommet. Which will allow the connection of the coaxial cable with the exterior of the box obstructing the entrance of fluids.

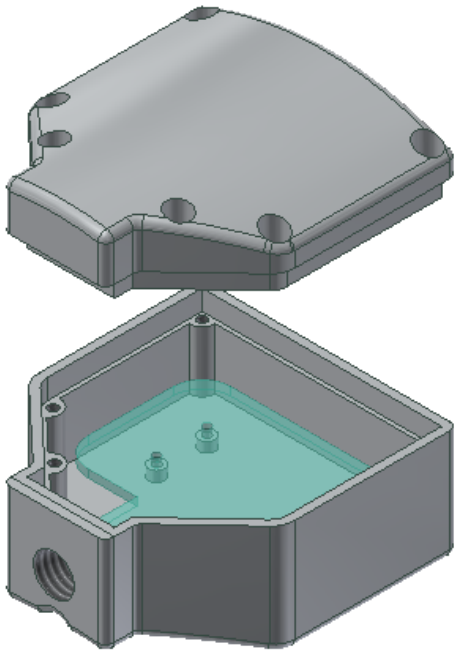

Figure 4.3: Housing Autodesk Inventor model Design

CAD files were used to produce the 3D printed parts, as shown in figure 4.4. The 3D printed pieces were fabricated in material that is magnetic compatible, as well as the gland, grommet and screws.

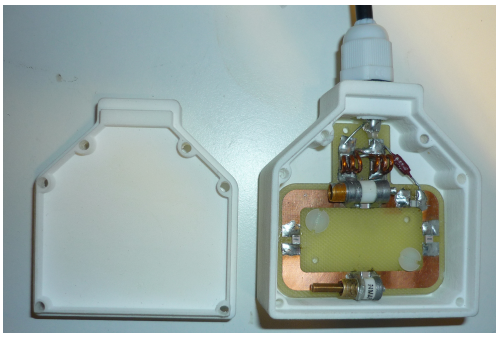
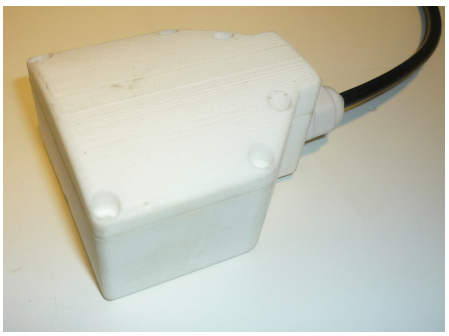

Figure 4.4: ASL coil and ASL coil housing

4.1.2 Tuning and Matching

According to the theory described in Chapter 2 to excite and detect a specific nucleus a RF pulse at the Larmor frequency of the nucleus must be applied. Resonant frequency of operation for which a RF coil is required to be tuned when used at magnetic field of magnitude 9.3844419T for the ^1H nucleus was computed according to equation 2.1. Coil is tuned to the following resonant frequency:

$$\mathbf{f_1 = 399.552MHz}$$

Circuit tuning to the required frequency is accomplished using three distributed capacitors. The capacitance is split on the circuit in order to get lower electrical length of the conductor which must be less than $\lambda/20$ when operating at high frequencies. Capacitance distribution also prevents radiation of the electric field from the coil. This methodology prevents the coil from behaving as an antenna.

However this methodology introduces resistive losses due to solder joins and resistance from capacitors, moreover it might disrupt the structure if capacitors are not properly solder. Care must be taken when soldering capacitors, soldering must be executed at high temperature (240°) and the joins must be well soldered with an uniform and shiny solder join. Solder joins with low quality will be a major factor to lower quality factor.

The tuning and matching process was developed under the following process.

In order to find tuning capacitance value to this coil geometry, a single capacitor with a value close to the estimated value of tuning capacitance was connected in the milled PCB in the central gap corresponding to C_2 in Figure 4.1. The other gaps of the circuit were closed using copper connections. The inductance of the coil can be calculated since the capacitance value is know and the resonant frequency of the coil is measured using the

shielded double loop probe which is connect to the network analyser performing $S21$ measurements. From equation 2.15 the inductance value computed is $L = 80.9539nH$. Applying the same equation, since the inductance value is constant in a certain loop shape the tuning capacitance was calculated, the final value is $C_T = 1.96pF$.

The new capacitance value was soldered on C_2 gap using parallel capacitance in order to have the required tuning capacitance since capacitor values between $1.8pF$ and $2pF$ were not available.

The unloaded and loaded Q of the coil was measured using HP network analyser. All the measurements performed, were performed with the coil inside coil housing.

The loaded measurements are performed using the test phantom. Measurements were made in $S21$ mode. At f_1= 399.552 MHz, $Q_{unloaded} = 280$ and $Q_{loaded} = 50$.

A match capacitor was soldered in the match capacitance gap C_4. The behaviour of the coil after addition of matching capacitor was measured. The measurement is done to evaluate the matching impedance between the coil and the coaxial cable, in order to perform measurement a coaxial cable is connected to the coil. The coaxial cable was then connected to the network analyser and measurements of the matching impedance were performed in $S11$ mode. To achieve a correct match the impedance observed in smith chart has to be close to 50 Ω at the resonate frequency. Measurements performed in $S11$ require a calibration of the network analyser to the end of the cable that will be connected to the coil.

The tuning capacitance was adjusted again after measuring the impedance match to the correct frequency and checked in the $S21$ mode in the network analyser. After this iterative process tuning capacitance was distributed to the gaps of the coil. In gaps C_1 and C_3 capacitors were chosen to have the same value and C_2 and C_4 were changed until a tuning and matching was achieved. In both gaps trimmer capacitors were soldered in parallel to a fix capacitor, these variable capacitors allow adjustment of capacitance, which enables a change in loading sample while the coil still resonates at the resonant frequency.

Final value capacitors are:

$$\mathbf{C_1 = 6.8pF; C_2 = 10pF + (1 - 33)pF}$$

$$\mathbf{C_3 = 6.8pF; C_4 = 15pF + (1 - 33)pF}$$

The minimum total capacitance value is $C_{Total} = 2,1pF$, in theory this value will correspond to a resonant frequency of 386.000 MHz however in practice the value is higher. Due to a resonant shift associated to the saline

phantom and volume coil load, the coil will in fact have a resonant frequency above 399.552 MHz when not loaded in order to achieve the required resonant frequency when loaded.

4.1.3 Active tuning circuit

Imaging protocol consists of several imaging techniques applied to the subject during a period of time. There are advantages in using RF coils which permits active tuning, using a detuned transmit coil that only transmits when is actively tuned. A detuned coil will prevent coupling with the volume coil, coupling would increase noise in images produced by the volume coil and would increase the risk to reach a SAR level above the allowed limit.

In the present methodology a PIN diode was placed in series in the coil circuit, PIN diode is represent by letter D in figure 4.1.

Using this methodology the coil is detuned when not biased, when the DC bias current is applied to the circuit, the PIN diode acts as a short circuit closing the circuit, the current can then flow the circuit.

To feed the diode with the DC current, an RF choke inductor is placed between the coaxial cable and the cathode of PIN diode. The RF choke also provide blocking the RF current from leaking to the coaxial cable which protect the interface hardware during RF transmission. To have bias voltage across PIN diode on the anode point DC bias comes from L_2 since DC does not flow over capacitors.

The DC bias is provided from a PIN diode driver in-house developed that will be described in section 4.3.

After tuning and matching the coil to 399.552 MHz and 50Ω a non-magnetic PIN diode with is soldered between C_3 and C_4. When the PIN diode is introduced in the coil care must be taken about the temperature of soldering, the PIN diode is a small device sensitive to high temperatures, in order to preserve the high quality of the PIN diode it must be soldered at a low temperature (230°) and once the diode is soldered it should not be moved again. After connection of the pin diode, the resonant frequency of the coil was assessed using S_{11} measurements to assure that the amount of capacitance introduce in the coil does not interfere if the total capacitance, coil capacitance was adjusted using the variable capacitors. The tuning and detuning capabilities were then observed using the network analyser.

4.1.4 Balun

A coaxial cable is an unbalanced device that feed RF current to the balanced device the RF coil. To ensure the balance of the current flowing in the coil a

balun was constructed, as previously described a device that can transform signals from balanced and unbalanced devices. In this project a lattice balun was constructed on the coil input. The balun design is shown in figure 4.5.

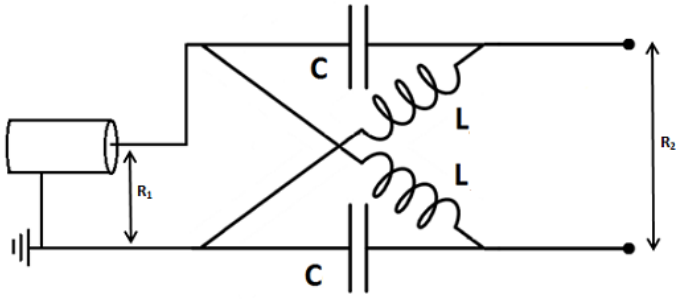

Figure 4.5: Balun circuit

The capacitance and inductance values are computed according to the following relationship:

$$X_L = X_C = X_M \Leftrightarrow \frac{1}{C\omega} = L\omega = \sqrt{R_1 R_2} \tag{4.1}$$

Where C and L are the capacitances used in the Balun, ω is the frequency in this case 399.552 MHz, R_1 is the resistance of the coaxial cable, in this case the cable and the interface hardware has a 50 Ω impedance. R_2 is the resistance in the surface coil, in this case as described before the coil is matched to a 50 Ω impedance. According to the previous values inductance L is $L = 19.9nH$ and and capacitance C is $C = 8pF$.

In the coil gaps represented in figure 4.1 as C_5 and C_6 two capacitors were placed in parallel, with values

$$\mathbf{C_5 = C_6 = 1.2pF + 6.8pF}$$

. Two inductors were custom built, sizes of the inductor were first estimated using an online calculator. The inductor was built from copper wire (1.25mm diameter), to construct the inductor wire was wrapped around a cylindrical object with 5.5mm diameter, final inductor had three loops. The cylindrical object was introduced inside the inductors and were soldered parallel as shown in figure 4.5.

Balun was tested using the test bed, monopole antenna and current probe described in section 3.4.

To test the balun the coaxial cable attached to the coil was fixed on the extremities of the test bed. Wood pieces with the same hight were split under the cable to provide stability. At the end of the cable , the cable was

wrapped around a ferrite ring to absorb cable currents. A current probe was placed around the cable and connected to port 2 of the network analyser. A monopole antenna, that induces common mode currents, was fixed to the plastic table near to the RF coil in test and connected to port 1 of the network analyser.

To have the balun at the resonant frequency the space between the loops of the inductors were adjusted in both inductors until the drop in the S_{21} measurement was at resonant frequency.

4.1.5 Cable Trap

Suppression of cable shield currents is an important procedure to better coil efficiency and to ensure safety requirements are meet.

Currents can be induced on the shield of the coaxial cable when a coil is not well balanced, other coils induce currents on the cable or it can arise from other sources. These currents can ultimately turn a coaxial cable into a radiative antenna. To suppress these currents a high impedance circuit must be added to the coaxial cable, the circuit is placed in a length below the characteristic quarter wavelength of the frequency. The wavelength λ at 400MHz is 75 cm.

A high impedance circuit is achieved, building a parallel LC circuit a blocking impedance is produced at the frequency of resonance. These type of circuits are named trap circuits. A cable trap can be clamped around the cable or be connected in series with the cable, in this project the second topology was adopted.

Capacitance and inductance values were estimated from simulations performed in QUCS, from the studied values the size of the trap was then decided. A PCB was design and milled as shown in figure 4.6. The PCB structure has dimensions 30mm x 15mm, cooper width of 5.6mm. A hole was drilled in the middle of the PCB permitting the positioning of an inductor.

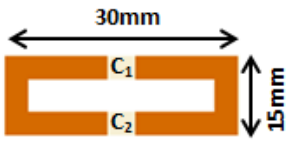

(a) PCB cable trap schematic

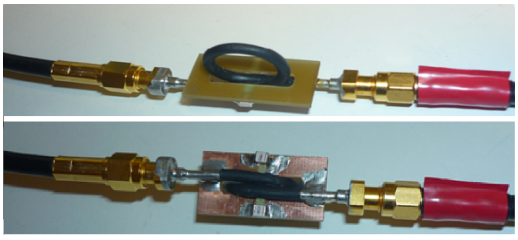

(b) Cable trap: top and underside

Figure 4.6: Cable trap

The balun consists of a single loop inductor of semi-rigid coaxial cable, 15mm diameter, the inductor was soldered on the extremities of the PCB and SMA connectors were soldered on each side of the coaxial cable. A capacitor was soldered on in each gap, the final capacitor values were:

$$\mathbf{C_1 = 1.8pF; C_2 = 2pF}$$

Balun was tuned to the resonant frequency using the test bed and two current probes connected to the network analyser. The balun was connected in each side to coaxial cables. Coaxial cables were fixed on the extremities of the test bed and wood blocks were place across the cable to provide a stable cable. To absorb the currents at each side of the cables, ferrite rings were wrapped around. In both sides current probes were placed around the cables, one probe was connected to port 1 of the network analyser and used to transmit signal, other probe was connected to port 2 and used as a detecting probe. Although the inductor is placed in a tight hole moving the semi-regid coaxial cable changed the inductance and balun was set to resonate at resonant frequency.

4.2 ASL labelling coil: Results

Coil performance results are evaluated using network analyser functions. A well designed and developed device which presents high performance results will in principle be traduced in a device high quality device when under practical use. Care must be taken to measurement conditions. Phantoms used must mimic as best as possible the real conditions, as well as the environment which should have the same conditions as it will have in the magnet room. Measurements were perform on a plastic table as far as possible from magnetic components and using the phantoms described in section 3.5.

4.2.1 Tuning and matching

Coil was connected to the network analyser through a coaxial cable and network analyser was set to perform S_{11} measurements. To perform better S_{11} measurements the system is first calibrated which will take in account coaxial cable length. The coil was loaded with the test phantom placed on the coil to mimic real conditions. Figure 4.7 shows that the coil is tuned to the resonant frequency and is matched to 22 dB at 399.552 MHz. A coil is well matched when match is above 20 dB. A smith chart is also presented. In a smith chart at the referential point it is indicated the transmission line impedance match in this case corresponds to 50 Ω. In this particular match

situation coil was not at the perfect match conditions (44.36 + j 5.67). This could be due to the loading situation, this situation means that some of delivered power will not be received.

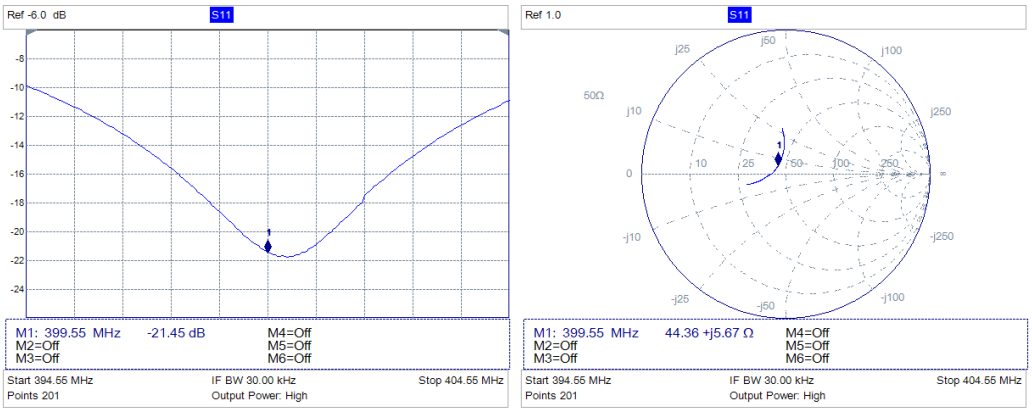

(a) S11 measurement in a log scale: tune and match

(b) S11 measurement in a smith chart showing coil matching

Figure 4.7: S11 measurements: tune and match

4.2.2 Active tuning

Detuning coil performance was assessed using both S21 and S11 measurements.

To perform S11 measurements the coil needs to be attached to a pin diode driver and to network analyser's port 1. To be attached to both devices the coil is connected to the RF+DC port of a bias tee that was developed and will be described in a posterior chapter. This allows the coil to be tuned and detuned and also a RF signal can be provided.

A single probe described in section 3.4 was attached to the network analyser's port 2, the coil was used to detect the signal transmitted by the coil which was attached to port 1 as described above. A S21 measurement was performed and the results are shown in figure 4.8a. In figure 4.8a the red trace shows coil tuned at resonance frequency and blue trace shows coil detuned. RF coil was 20 dB detuned. In figure 4.8b S11 measurements also showed the detuning performance of the coil. In this case red trace shows the coil detuned and blue trace shows the coil tuned. Detuning/tuning was successfully achieved.

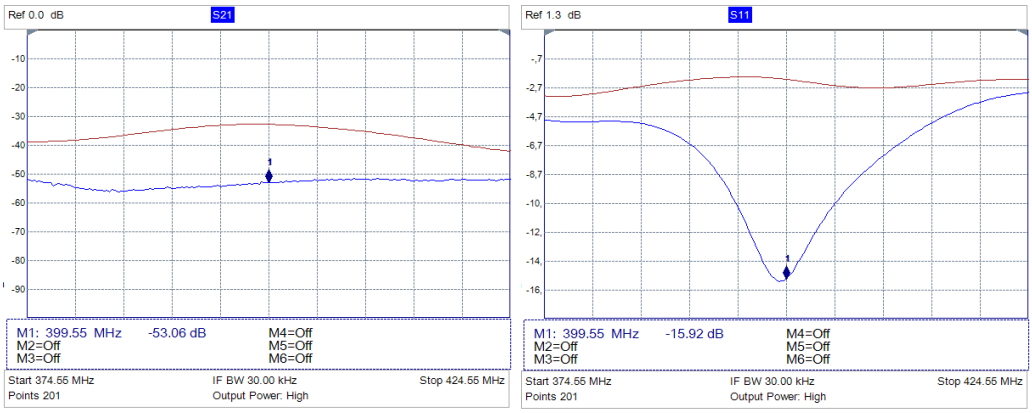

(a) S21 measurement:Red trace- coil tuned; Blue trace-coil detuned

(b) S11 measurement: Blue trace-coil tuned; Red trace- coil detuned

Figure 4.8: Coil detuning network analyser's measurements

4.2.3 Balun

As described in balun methods section, a current probe was connected to port 1 of the network analyser and an antenna was connected to port 2 of the network analyser. In figure 4.9 the blue trace shows the balun tuned at the resonant frequency.

To measure the quality of a balun the ratio between the differential mode gain to the common mode gain is calculated. This is called the common mode rejection ratio (CMRR). To calculate the ratio the balun must be short-circuited to access the common mode gain, which was achieved by bridging the balun. This is represented by the red trace. CMRR value was grater than 15dB.

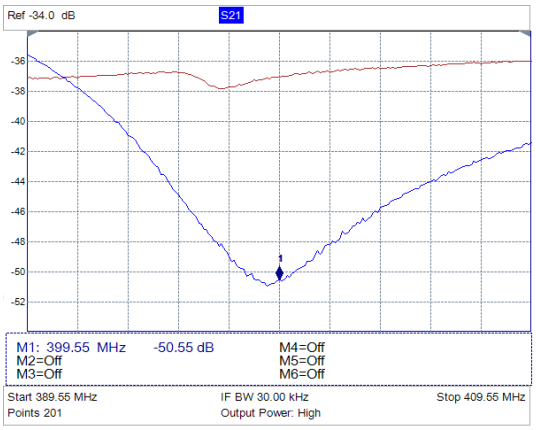

Figure 4.9: S21 measurement: Blue trace- Balun active; Red trace-Balun inactive

4.2.4 Cable Trap

$S21$ traces were acquired to evaluate the performance of the cable trap. As observed in figure 4.10 cable trap was successfully tuned to the resonant frequency which corresponds to blue trace. The ratio of shield current that was attenuated is calculated. The value is the result of subtraction of the $S21$ measurements when the balun is active and inactive. The inactive balun trace corresponds to the red trace. The value calculated to this cable trap is 20 dB.

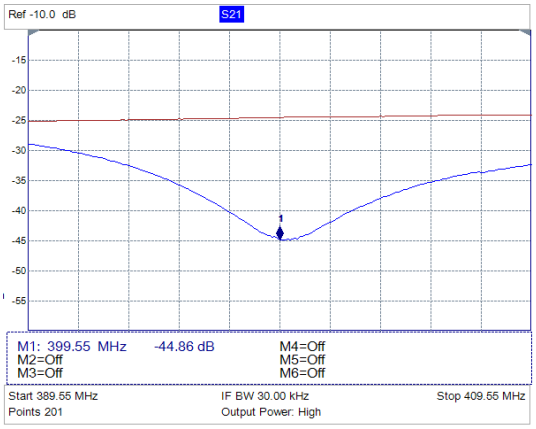

Figure 4.10: S21 measurement: Blue trace- Cable trap active; Red trace-Cable trap inactive

4.3 Pin Diode Driver

In previous sections it was described the detuning properties of the ASL coil. To switch between tuning and detuning states PIN diode impedance states must change. A PIN diode driver is a device which controls PIN diode behaviour, pin diode driver itself is controlled by a TTL signal (0-5V) activated by the MRI system. A PIN diode driver was constructed as shown in figure, circuit design was based on [34].

In the circuit the driver turns the TTL signal into a bias signal due to the use of transistors. A low TTL signal is traduced in a reversed bias diode, while a high TTL signal forward bias the diode. The final current is defined by the current limit resistor and the inductor is used to protect the pin diode driver from RF currents. LEDs are used in this circuit to give information about the detuning state of the coil.

Circuit was designed using Kicad software and was then CNC milled. All the components were carefully soldered on the PCB board. BNC connectors were added to the board to allow TTL input and current signal output.

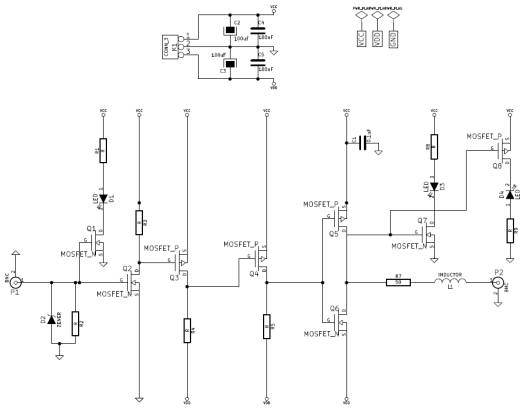

Figure 4.11: Pin diode driver circuit

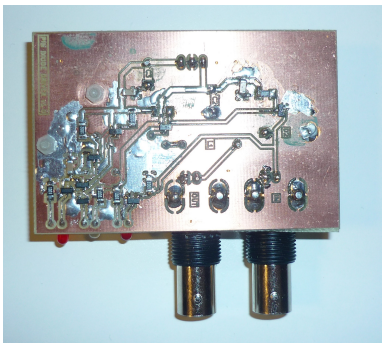

Figure 4.12: PIN Diode driver

4.4 Bias tee

A bias tee is a device that allows injection of DC power into an RF circuit with no effect on the RF signal which is useful when a DC and a RF signal have to share the same coaxial cable. In this project a bias tee was used to apply the DC bias signal from the pin diode driver previously described into the ASL coil circuit to tune/detune the coil.

A bias tee has three ports designed in the shape of a T. Figure 4.13 shows a schematic circuit of a bias tee. As it is shown there is a port labelled **DC**, where the DC bias signal is applied and the RF signal is applied at the port labelled RF, both powers are applied to the device through the **RF+DC** port. Capacitors block DC current and pass alternating current for that reason a large value capacitor is placed between **RF** and **RF+DC** blocking the DC signal from flowing through the RF path. To block the RF signal, a parallel LC circuit resonating at the resonant frequency bandwidth is placed in between the **DC** and **RF** ports blocking the **RF** current. The capacitor between **DC** path and ground routes any RF that may leak to ground [14].

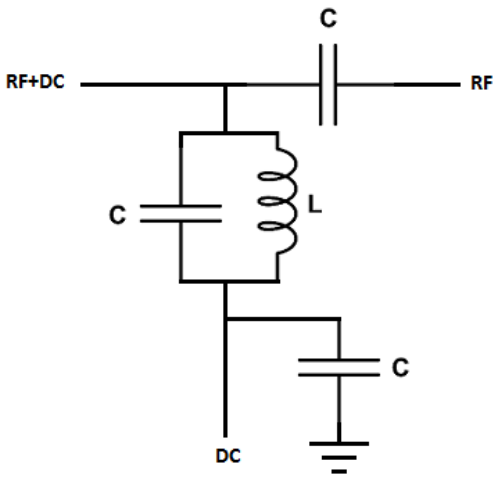

Figure 4.13: Bias tee circuit

4.4.1 Methods

A bias tee was constructed following the above circuit scheme using microstrip circuits technique. A microstrip width has a specific value, based on the characteristic impedance and on the specificities of the PCB board. A PCB constructed from 1.6mm thick double sided copper clad FR-4 with 50 Ω characteristic impedance corresponds to a 3.1mm microstrip width. To ensure this impedance the gap between ground and strip on the top layer is 4.65mm (1.5mm x 3.1mm). The black circles corresponds to vias used to connect ground planes. According this specifications a bias tee PCB was CNC milled.

A high voltage high value capacitor was soldered in C_1 position, final value was 471pF. The same capacitance value was connected in C_3 position. To construct the LC trap an 3 loop with 4.5mm inner diameter inductor was built from 1mm cooper wire, inductor was soldered in parallel with a 5.6pF capacitor.

PCB was enclosed in an aluminium box with holes where a BNC connector and 2 SMA connectors were inserted and soldered to connect with the respective cables.

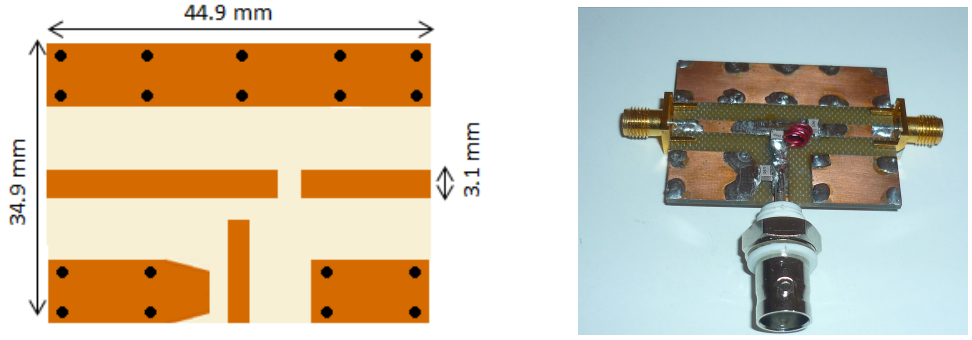

(a) PCB bias tee schematic

(b) Bias tee

Figure 4.14: Bias tee: schematic and photo

4.4.2 Results

Figure 4.15 shows the network analyser traces (S21) for the performance of the bias tee. Blue marker shows the value measured at 399.552 MHz.

Figure 4.15a shows that there is an attenuation of 54.80 dB between DC port and RF port at 399.552 MHz which is a reasonable level of attenuation. The insertion loss (the lost signal due to introduction of a device in the transmission line) between the RF port and RF+DC port was 0.28dB.

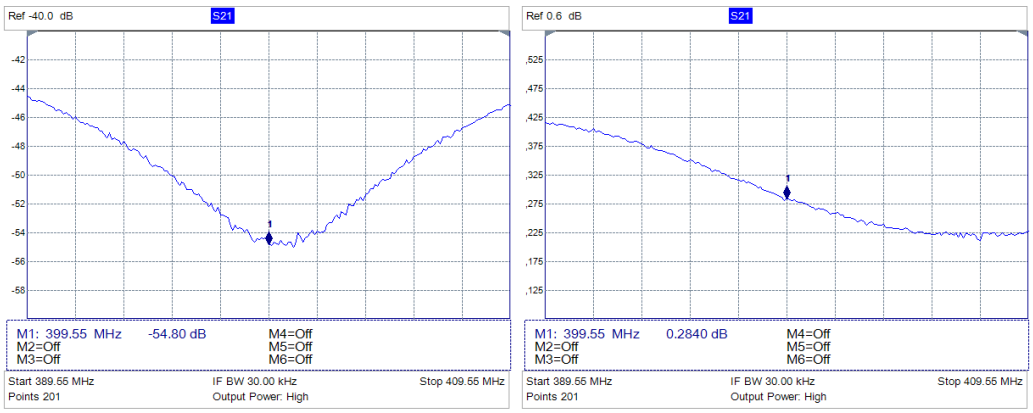

(a) Isolation (S21 measurement) between RF and DC Port

(b) Insertion loss (S21 measurement) through RF to RF+DC

Figure 4.15: Bias Tee performance

4.5 Conclusion

The goal of this chapter was to design and construct an ASL labelling coil, with active decoupling ability, providing methods to minimize common mode currents. A coil housing designed according to the specificities of the experiment was also requested.

The RF transmit coil was successfully constructed. The coil provided a match of 22dB for the requested resonant frequency (399.552 MHz). Active tuning was achieved, with a difference of 20 dB between the tuned and detuned S21 measurement. The two balancing methods provided 15 dB of common mode rejection ratio for the balun while the shielded current was attenuated by 20dB at 399.552 MHz. A coil housing suitable for the experiment was designed.

Moreover two other devices were constructed: a pin diode driver which was successfully used to tune the ASL labelling coil and a bias tee that allowed a isolation between the RF and DC port of 54.80 dB with a low insertion loss (0.28 dB).

Chapter 5

Sodium transmit/receive coil

Several imaging protocols can be performed to study the neurophysiology changes in brain HI injury. Although sodium imaging has much lower SNR and resolution than proton imaging sodium MRI imaging has proved to provide relevant informations. In addition to the development of the ASL coil, a transmit/receive sodium coil suitable for newborn piglet brain imaging was developed. The aim of the project was to verify the potential of sodium imaging as complementary diagnostic tool in brain HI injury.

The following chapter describes the experimental procedure followed to develop a transmit/receive surface coil for sodium imaging, methods and results are presented.

5.1 Sodium labelling coil: Methods

As discussed in section 2.2.7 higher SNR is obtained when a surface coil is used. Due to this fact a single tuned surface coil was built. As also discussed in section 2.4 it is useful to include proton imaging capabilities to match the anatomical information along with sodium imaging data.

In this project a proton volume coil (section 3.1) was used to provide anatomical information. The constructed surface coil is placed on the piglet's head surface and inserted in the volume coil. When coils that work at different resonant frequencies are used in conjunction a mean to avoid coupling between coils must be design.

The description of the methods related to coil circuit and housing design, methods related to tank circuits and remote tuning are presented. At last tuning and matching and balun set up values are described

5.1.1 Design

5.1.1.1 Circuit design

The circuit design for the ^{23}Na coil is shown in figure 4.1.

Circuit configuration consists of 6 capacitors ($C_1 - C_6$) distributed in series in a rectangular path circuit. A tank circuit consisting of an inductor L_{Trap} and a capacitor L_{Trap} is placed in series in between two capacitors for decoupling. A remote tuning box was added to the circuit. A lattice balun consisting of two capacitors (C_7, C_8) and two inductors (L_1, L_2) is presented.

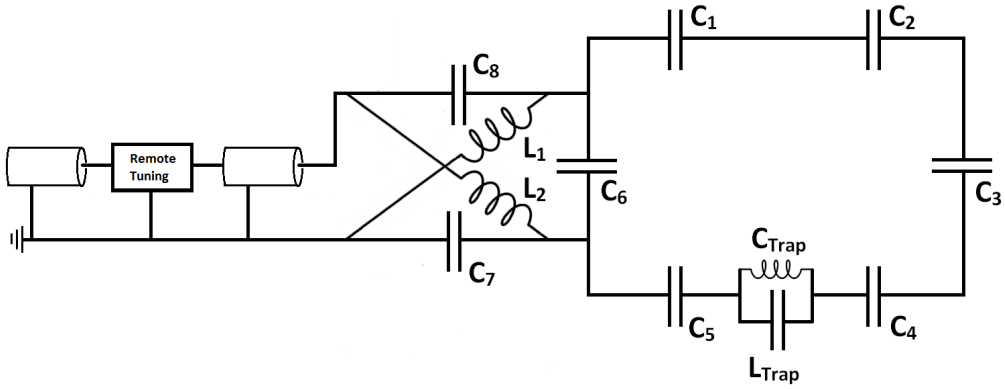

Figure 5.1: ^{23}Na coil circuit

The coil has a rectangular shape as shown in Figure 5.2, with dimensions ($82mm \times 110mm$), with a track width of 5.6mm. The dimensions of the coil are compatible with piglet brain, the cooper track has 8 gaps milled in order to allow a distribution of capacitance.

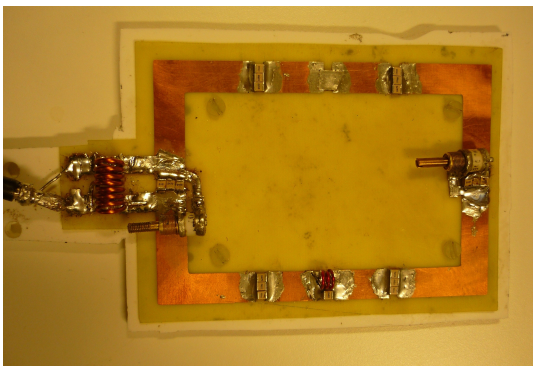

Figure 5.2: ^{23}Na coil

5.1.1.2 Mechanical Design

Operating without the housing provided good flexibility, but is not a robust long-term solution; preferably a more compact, better suited housing should be implemented.

Housing provides better protection of the coil while also preventing the excess of loading. During the experiments coil was not placed in a conventional housing it was placed on an acrylic board which allow a distance between surface and the coil.

However a long-term solution for coil housing was designed using Autodesk Inventor software to posterior 3D printing, as presented in Figure 5.4.

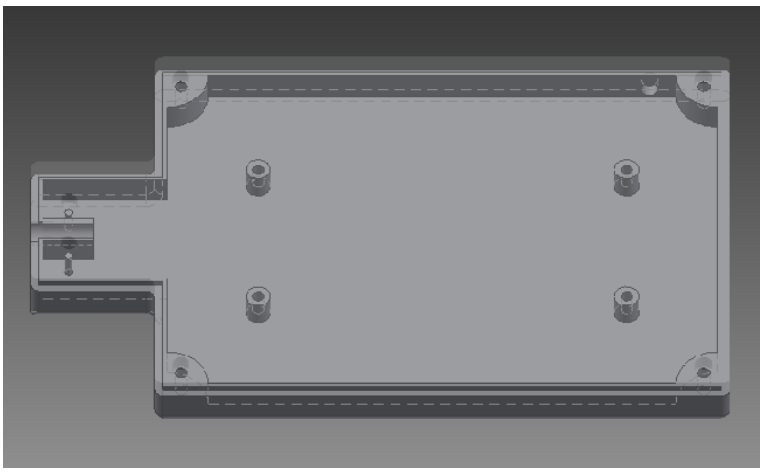

Figure 5.3: 3D model of ^{23}Na coil housing

5.1.2 Tank Circuit

To overcome the possible coupling between ^{23}Na coil and ^{1}H coil a tank circuit was implemented in series with the coil. Sodium frequency is almost 300 MHz far from the proton frequency, a parallel LC circuit implemented in the low frequency coil resonating at the frequency of resonance of the volume coil enables the coil blocking induced currents at the ^{1}H frequency. Note that this trap will open coil circuit at the frequency 399.552 MHz but does not stop the ^{23}Na from having a shift in resonance when placed inside the volume coil.

This trap consisted of an inductor and a capacitor in parallel placed in series in the coil circuit in between capacitors C_4 and C_5. LC trap values were simulated in the QUCS simulator to verification of L and C range values. A trap was first constructed out of the coil, in order to do this the cable used

have to be carefully calibrated. An inductor with a 5.8mm radius with 3 loop was constructed from 1mm copper wire was soldered with a 4.7pF capacitor in parallel.

The trap was setted up in the circuit in place with other gaps opened, impedance magnitude measurements (S11 measurement) of the trap was performed on network analyser, adjustments were done to the gaps of the inductor until the magnitude impedance value was greater than $10k\Omega$ at 399.552 MHz.

5.1.3 Remote tuning

When coils are placed inside the magnet bore and confined to small volumes moreover with different loading conditions from the ones where they were tested tuning and matching vary from the values observed in the bench measurements. Poor match and resonance shifts decrease image quality and sensitivity so many techniques are used to allow varying tune and match.

The easiest way is to properly tune and match the probe is adding variable capacitors. However this manual manipulation on the coil is not always possible due to limited space such as small bores, extra volume coils or extra hardware. In many situation one easy solution is to use fiber rods (magnetic compatible components) as an extension of the capacitors. Although possible is not always effective and other solutions may be performed.

One such solution is to tune and match the coil outside the coil area outside the magnet bore where space is not a problem. The match box circuit is shown in figure. To build this circuit the coil is intentionally mistuned for 2% to 5% and the remote box is add to the transmission line. The transmission line must be nλ way from the coils, it is preferable to be as close as possible but out of the bore.

Articles such as [49] and [20] present results using different configurations and a good review on remote tuning and other coil's construction methods can be found in [53].

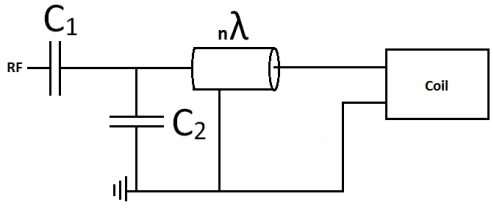

Figure 5.4: Remote tuning circuit

A remote circuit box was constructed however due to safety issues and a lack of capacitors with range of values needed the box was not used on the experiments. A remote coil matching network (Doty Scientific, Inc.) was used in this experiment.

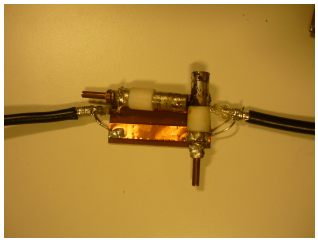

(a) Experimental remote matching network

(b) Remote coil matching network

Figure 5.5: Remote boxes

5.1.4 Construction process

Tuning and matching of this circuit was performed in two stages, first the coil was tuned to the ^{23}Na resonant frequency and after it was mistuned, a mistuning of about 3%.

According to equation (2.1) the resonant frequency required to a ^{23}Na placed in a $9.3844419T$ external magnetic field was computed.

Coil is tuned to the following resonant frequency:

$$\mathbf{f_1 = 105.683MHz}$$

The process of construction the coil is similar to the process described in section 4.1.2, methods followed are similiar as well as the justifications to the procedures.

A gap of the PCB was connected with a single capacitor in order to find the resonance frequency of the coil. The inductance of the coil calculated (equation (2.15)) was $L = 179nH$ and the final tune capacitance was computed $C_{tune} = 12.6pF$.

The unloaded and loaded Q of the coil was measured using HP network analyser. The loaded measurements are performed using the test phantom. Measurements were made in $S12$ mode. At f_1= 105.683 MHZ, $Q_{unloaded}$ = 320 and $Q_{loaded} = 54$.

The match capacitor C_{match} was soldered in the match capacitance gap, C_6 and coaxial cable was soldered to the coil. Matching measurements were performed in $S11$ mode of the network analyser. The tuning capacitance was

adjusted again after measuring the impedance match to the correct frequency and checked in the $S12$ mode in the network analyser. Tuning capacitance was then distributed over the five gaps of the coil. In each gap 3 capacitor were soldered in parallel. One of the capacitors is a trimmer capacitor with $1 - 33pF$ variable capacitance, placed in C_1 to allow better tuning capacitance.

In order to achieve a balanced circuit a lattice balun was placed on the coil. The balun consists of two $15pF$ capacitors placed in parallel and two inductors across the capacitors. Inductors with 8.3mm radius and four loops were constructed from 1.5mm cooper wire. The same circuit as in section 4.1.4 was performed and the balun was setted up in the same conditions.

After complete coil construction images performance bench measurements and test images were performed. It was concluded that tune and match was difficult to perform on the coil.

The chosen solution was to implement remote tuning. In order to add the tune box the coil was mistuned around 3%. Connection between the coil circuit and the balun was desoldered and capacitance values were changed until the resonating frequency reached the desired frequency 102.4 MHz measured on network analyser S21 mode using the double loop probe.

Final capacitors values were:

$$\mathbf{C_1 = C_2 = C_4 = C_5 = 47pF + 5.6pF + 3.9pF}$$

$$\mathbf{C_3 = 100pF + 22pF + 10pF + (1 - 33)pF}$$

$$\mathbf{C_6 = 100pF + 47pF + 47pF + (1 - 33)pF}$$

5.2 Sodium transmit/receive coil: Results

Coil performance results are evaluated using network analyser functions. Measurements were performed using the test phantom and on a plastic table as far as possible from magnetic components and using the phantoms described in section. Measurements were also performed inside the volume coil and inside the magnet room.

5.2.1 Tuning and Matching

The coil final resonating frequency is measured by performing an S21 measurement. Figure 5.6a shows coil resonance when the coil is not loaded and figure 5.6b when the coil is loaded. Since the coil was de soldered from the

coaxial cable the resonant frequency is approximately 97% of 105.683 MHz As expected the signal drops as a result of the loading.

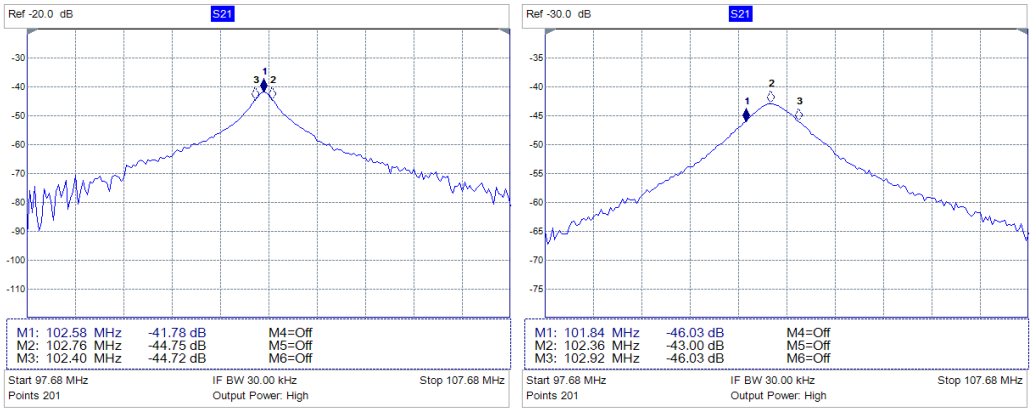

(a) S21 measurement: unloaded coil **(b)** S21 measurement: loaded coil

Figure 5.6: Coil tuning measurements

According to measurements on S11 mode performed on the logarithmic scale a reasonable tune and match of the coil was achieved, -27.52dB at 105.68 MHz, observing smith chart presented in 5.7b match value was near 50 Ω, the value was 53.59+j2.47Ω.

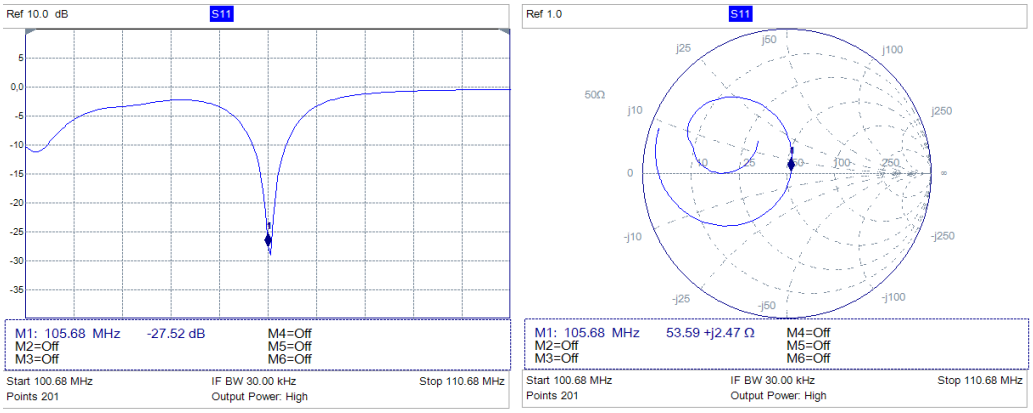

(a) S11 measurement in a log scale: tune and match **(b)** S11 measurement in a smith chart showing coil matching

Figure 5.7: S11 measurements: tune and match

5.2.2 Balun

As previously described, a current probe was connected to port 1 of the network analyser and an antenna was connected to port 2 of the network analyser. In figure 5.8 the blue trace shows the balun tuned at the resonant frequency.

The CMRR was calculated as in section 4.2.3 the value was grater than 15dB.

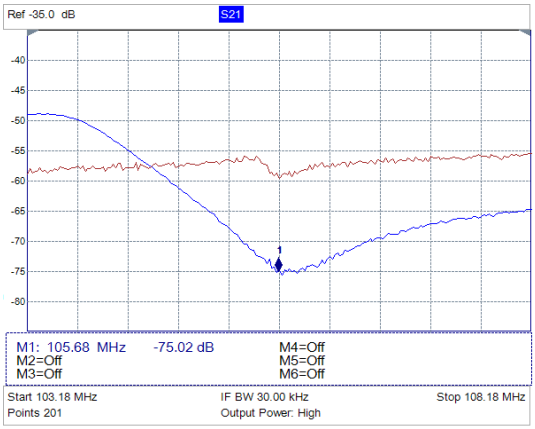

Figure 5.8: S21 measurement: Blue trace- Balun active; Red trace-Balun inactive

5.3 Conclusion

The goal of this chapter was to design and construct a transmit/receive sodium coil resonating at 105.683MHz, decoupled at the proton frequency, providing methods to minimize common mode currents. A coil housing designed according to the specificities of the experiment was also requested.

The transmit/receive sodium coil was successfully constructed. The coil achieved a match of 27.52dB at 105.683MHz, to allow better tuning and matching to the different subjects it was added a remote tune box to the feeding coaxial cable and necessary changes were done on the coil circuit. Moreover it was installed an LC trap as mean of decoupling to the proton frequency. The balun installed on the coil provided 15dB of common mode rejection ratio.

The coil housing was designed according to the requirements.

Chapter 6

Sodium transmit/receive coil imaging

To evaluate the transmite/receive surface coil multiple phantom and in vivo images were acquired. Imaging was performed on the 9.4T Varian system and data was loaded and analysed (signal analysis, intensity versus depth histograms and signal-to-noise ratio calculation) using Matlab.

In all the following experiments, the T/R ^{23}Na surface coil was placed inside the ^{1}H volume coil, to be used as reference to the coil location and assess anatomical information. The coil position in relation to the magnet isocenter is also a measure to be aware, since near the isocenter there is better homogeneity so the surface coil must be in place with magnet isocenter.

6.1 Phantom imaging

Coil experiments were first performed in a phantom in order to investigate:

1 – Overall coil performance

2 – Sensitivity of the coil to different sodium concentrations

3 – Optimum acquisition parameters, such as TE, TR, flip angle, number of averages, to maximise signal-to-noise efficiency

To perform phantom images with different sodium concentrations a phantom was constructed as described in section 6.1.1.

6.1.1 Sodium imaging phantom

In order to observe if the transmit/receive sodium coil can image different concentrations of sodium, a phantom was constructed.

Three falcon tubes with 50 mL in volume were filled with 3 different concentrations of NaCl, the concentrations were 0.09%, 0.9% and 9%. The

falcon tubes were attached to a plastic cylinder bottle that was filled with 0.9% NaCl concentration. Two holes were drilled on the lid of the bottle and the bottle was then completely sealed and filled with water by the holes to avoid bubbles that if existent would decrease image quality.

Figure 6.1: ^{23}Na phantom

6.1.2 Imaging results

Following localization with the proton coil, sodium images of the phantom were acquired with 2D GRE sequence. The signal to noise ratio of the phantom images was calculated as

$$SNR = 0.66 \times \frac{meansignal}{noiseregionstandarddeviation}$$

0.66 is the Rayleigh distribution correction factor.[28]

Several images were performed with the following parameter changes:

TE=[2.7 5 7.5 10 20 30]ms, TR=100ms, Flip angle=130^o;

TE=2.7ms, TR=[6 10 15 20 50 75 100]ms, Flip Angle=130^o;

TE=2.7ms, TR=100ms, Flip angle=[30 60 90 110 130]^o. Images were acquired with: slice thickness= 20mm, acquisition matrix=64×64,FOV=100mm×100mm, 300 averages.

Sodium phantom images are shown in figure 6.2, axial orientation plane.

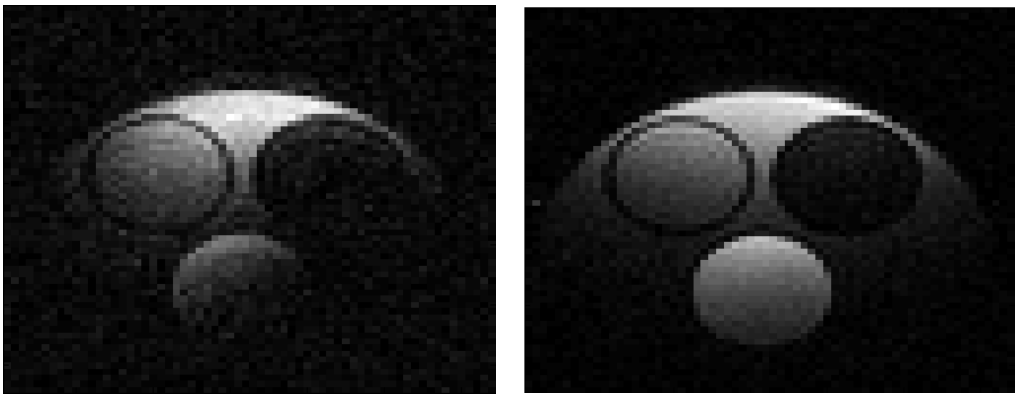

(a) Phantom imaging: TE=30ms; TR=100ms

(b) Phantom imaging: TE=2.7ms; TR=100ms

Figure 6.2: ^{23}Na Phantom imaging

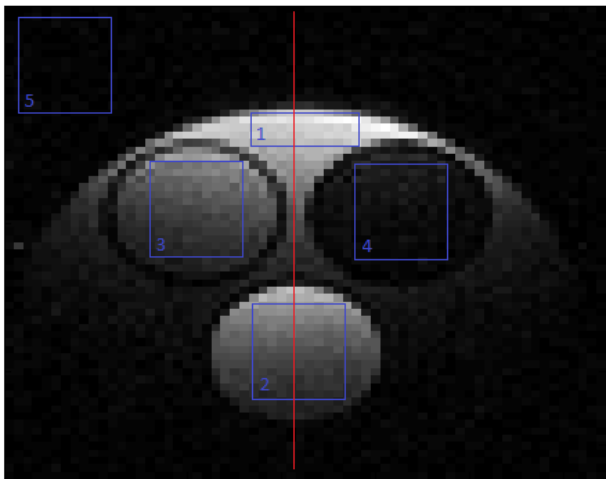

Figure 6.3: SNR regions

The SNR on signal region shown as 1 of figure 6.2a and 6.2b was calculated on matlab according to the function previously described. The calculated values were 23.92 to the image where the longer TE was prescribed and 44.74 was the value calculated to the shorter TE that was possible to achieve TE=2.7ms.

From all the images acquired with the different sets of values the best results were with the following parameters, TE=2.7ms, TR=100ms, Flip angle=130^o. As described in introduction sodium mri requires short TE values and long TR values, however with the sequences available it was not possible to acquire images with a shorter echo time. The other procedure to

improve the SNR is to select a considerable number of averages in this case 300.

The SNR of regions 1 2 3 and 4 was calculated. SNR in region 1=44,74; region 2= 20.79; region 3=21.30; region=4.53. Coil is not sensitive to low concentrations of sodium. Regions 1 and 2 are in different depths however SNR values are similar because the sodium concentration is very high the SNR is similar to the one in region 2.

In Figure 6.4 it is shown a chart that presents the signal intensity according to the depth in centimetres, chart corresponds to a line that in the image center represented in red in figure 6.3

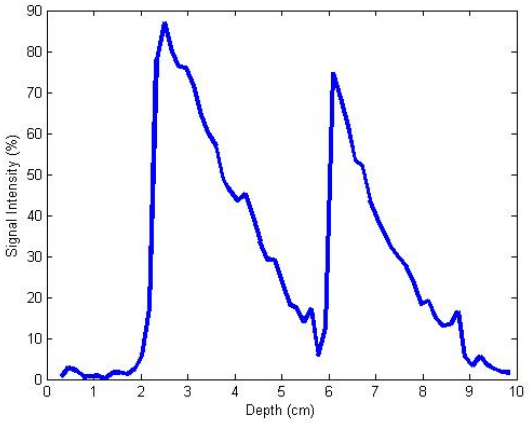

Figure 6.4: Signal intensity variation according to depth

The chart shows the signal decay of the image is shown. For a concentration similar to sodium concentration in vivo, the sensitivity was about 20mm. However due to a change in the sodium concentration the the signal significantly rose, for about 20mm. Although this concentration was used for phantom tests it is not an in vivo concentration.

In general as expected in a surface coil the signal intensity is higher at the surface of the coil.

6.2 In vivo imaging

6.2.1 Subject preparation

Animal experiments were performed in compliance with UK Home Office Guidelines (Animals [Scientific procedures] act, 1986). In vivo experiments were performed on term-born piglets 24 hours old which were firstly sedated

with intramuscular midazolam (0.2 mg/kg). Then, subjects were given isoflurane anesthesia(4% (vol/vol)), anesthesia was then maintained through the experiment, between 2% and 3%. Mechanical ventilation was performed. Maintenance and medicine fluid were administrated through an umbilical venous catheter. An umbilical arterial catheter ensures control of several blood parameters. All animals are also physiologically monitored.

Surgery is performed to isolate the common carotid arteries at the fourth cervical vertebra, then remotely controlled occluders encircle the arteries. These occluders are inflated to induce the hypoxic ischaemic insult. Piglets were placed in the pod previously described in prone position and immobilised.

6.2.2 Imaging results

In vivo experiments were conducted during the complex in vivo experiments that involved the piglet experiment. The aims of the in vivo imaging was to successfully perform sodium imaging in vivo investigating the different parameters that must be change in order to achieve better performance. Moreover this experiment was done to test different methodologies that could be done in order to evaluate concentrations and references, using the experimental set up.

The sodium transmit receive surface coil described in chapter 5 was positioned on top of the head of the piglet. Sodium MRI data was acquired before insult, 24 h and also 48 h after insult.

One of the constraints with a imaging protocol that comprises many types of imaging and in several days is the need to move the subject and move coils which ultimately changes coil position not allowing a correct comparison of images. In an attempt to overcome this problem two small fiducials were constructed with two NaCl concentrations 0.3% and 0.6%. These two plastic feducials were placed in holes drilled in nilon rods that were part of the pod set up. These tubes can be used as reference position points but also as reference of concentration.

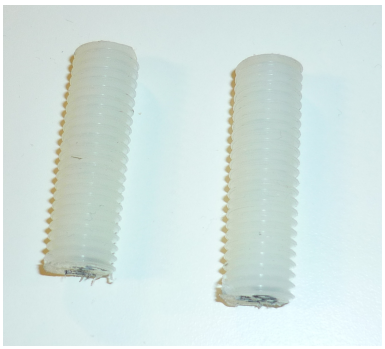

Figure 6.5: Tube phantoms

Figure 6.6 shown ^{1}H piglet brain images in the three planes to show the anatomical reference to the sodium images. Figures 6.7 shows ^{23}Na axial piglet brain images. The data set presented was acquired in the same piglet and in different days, before insult ,24 hours after insult and 48 hours after insult. The images were acquired with the 2D gradient echo sequence and the following parameters:TE=2.55ms,TR=100ms,flip angle=90°, averages=300, FOV=$6mm \times 10mm$, acquisition matrix=32×64, slice thickness= 20mm.

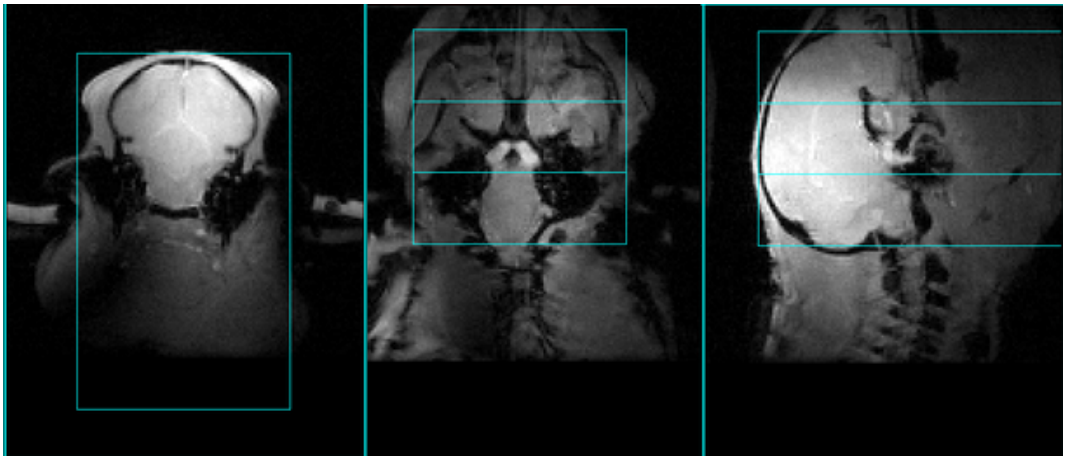

Figure 6.6: ^{1}H imaging: Anatomical reference: axial, coronal and saggital images of piglet brain

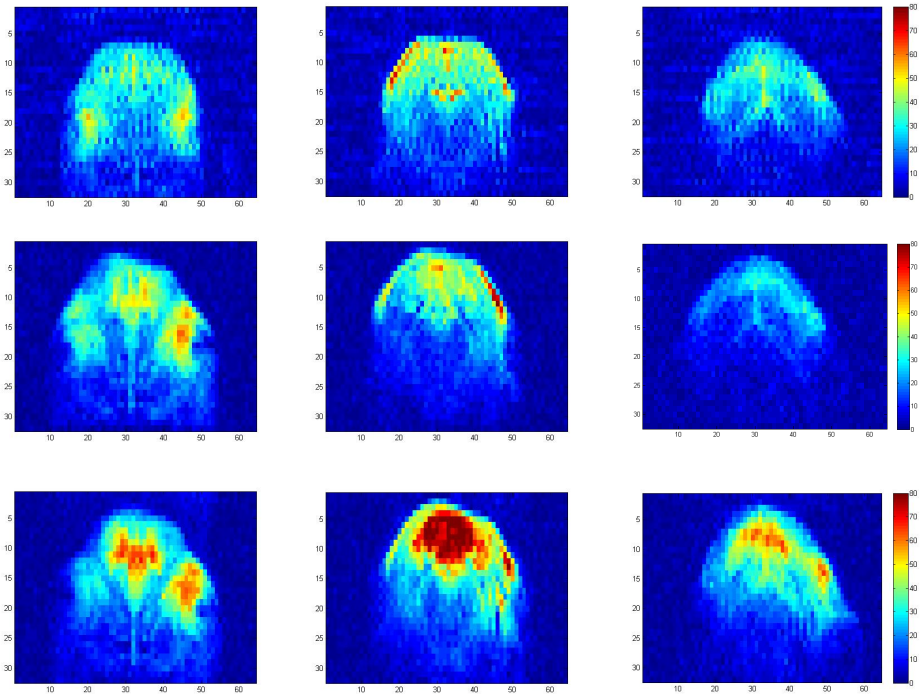

Figure 6.7: ^{23}Na images: Axial images of piglet brain. The three images shown in each row are different axial slices acquired at different positions in the piglet brain. Top images: before HI injury; Middle: 24 hours after insult; Bottom: 48 hours after insult

The axial ^{23}Na brain images shown acceptable SNR, varying between 10 and 20, when a high intensity region is chosen.The value is lower when compared to phantom SNR which was expectable due to different loading conditions. The spatial resolution covers a significant part of the brain however the attempted method to image the fiducials proved to be inefficient. Due to that reason it was not possible to proceed with the quantification analysis.

There is a noticeable difference in signal intensity between images from different days. A hyper intensity region is present in the second image of the 48 hour imaging set.

The ^{23}Na increase shown in the images of the 48 hour imaging set is consistent with previous results found in ischaemia models [22]. However it must be taken in consideration the limitations of the project. As explained before quantification of sodium concentration was not performed and the images can correspond to a different imaging are of the brain since the coil is removed and placed again to acquire the images.

6.3 Conclusion

The goal in this chapter was to test the transmit/receive sodium coil providing phantom and in vivo images.

The coil was tested on a phantom with different sodium concentrations. The acquisition sodium parameters were investigated and a maximum SNR on a region interest of 44.74 was achieved with a TE=2.7ms compared to a 23.92 with TE=30ms.

The in vivo imaging was performed before insult, 24 and 48 hours after insult. Sodium imaging was successfully performed, allowing recognition of different brain regions. By visual inspection it was possible to identify a region of high signal sodium intensity 48 hours after insult.

Chapter 7

Conclusion and Further Work

Two RF coils with different finalities for use at a 9.4T scanner were proposed:a coil to perform ASL RF transmission and ^{23}Na transmit/receive coil.

A transmit surface ASL coil was designed and tested. The coil was tuned and matched to the proton frequency at 9.4T and the appropriate bench test results were shown.

A coil presents two balance methodologies, a balun constructed in the coil and a cable trap.

As required the coil is actively tuned at the resonant frequency. A pin diode driver to switch the pin diode and a bias tee to connect the coil to the pin diode driver and the scanner system were also successfully constructed. The coil housing proved to be efficient since it seals completely the coil.

A transmit/receive surface coil was designed and tested. The coil was tuned and matched to the sodium frequency at 9.4T. The bench measurement results are presented. The coil has the advantage of remote tuning and matching which allows better tuning and matching without moving the whole set up.

The ^{23}Na coil was successfully tested on the MRI scanner with phantom and in vivo. ^{23}Na phantom images present good signal to noise ratio and different sodium concentration were distinguished. The initial ^{23}Na in vivo images allow the visualition of the main anatomical regions of piglets brain.

There are several improvements that can be performed in both cases. In the ASL coil it is necessary to proceed to the adequate imaging test which were not yet performed due to other hardware constrains. Phantom and in vivo images must be performed. In the ^{23}Na new coils should be constructed using the knowledge acquired with this coil.

^{23}Na imaging would benefit from a volume coil tuned at the resonant frequency. Doubled tuned coil, ^{1}H/^{23}Na is also a possible improvement, in this case the problems related with the anatomical reference images are mitigated

since both images are performed using a single coil. Apart from the hardware development changes acquiring images with different pulse sequences is recommendable even using the present coil. Since the T2 decay is very short, pulse sequences which allow the application of TE shorter than 1ms would bring considerable benefits to ^{23}Na imaging.

Bibliography

[1] Ian C Atkinson, Aiming Lu, and Keith R Thulborn. Clinically constrained optimization of flexTPI acquisition parameters for the tissue sodium concentration bioscale. *Magnetic resonance in medicine: official journal of the Society of Magnetic Resonance in Medicine / Society of Magnetic Resonance in Medicine*, 66(4):1089–1099, October 2011. PMID: 21446034.

[2] A. J. Barkovich, S. P. Miller, A. Bartha, N. Newton, S. E. G. Hamrick, P. Mukherjee, O. A. Glenn, D. Xu, J. C. Partridge, D. M. Ferriero, and D. B. Vigneron. MR imaging, MR spectroscopy, and diffusion tensor imaging of sequential studies in neonates with encephalopathy. *American Journal of Neuroradiology*, 27(3):533–547, March 2006.

[3] Robert Bartha, Ting-Yim Lee, Matthew J Hogan, Sarah Hughes, Enzo Barberi, Nagalingam Rajakumar, and Ravi S Menon. Sodium t2*-weighted MR imaging of acute focal cerebral ischemia in rabbits. *Magnetic resonance imaging*, 22(7):983–991, September 2004. PMID: 15288139.

[4] Ajna Borogovac and Iris Asllani. Arterial spin labeling (ASL) fMRI: advantages, theoretical constrains and experimental challenges in neurosciences. *International Journal of Biomedical Imaging*, 2012:1–13, 2012.

[5] C. P. Chao, C. G. Zaleski, and A. C. Patton. Neonatal hypoxic-ischemic encephalopathy: Multimodality imaging findings1. *Radiographics*, 26(Supplement 1):S159–S172, October 2006.

[6] Poskitt K Chau V. Magnetic resonance imaging in hypoxic-ischemic encephalopathy: Still a cool test. *Archives of Pediatrics & Adolescent Medicine*, 166(7):669–671, July 2012.

[7] David B Clayton and Robert E Lenkinski. MR imaging of sodium in the human brain with a fast three-dimensional gradient-recalled-echo

sequence at 4 t. *Academic radiology*, 10(4):358–365, April 2003. PMID: 12678174.

[8] Microsemi Corporation. The PIN diode circuit designers ' handbook. 1998.

[9] Arash Dabirzadeh and Mary Preston McDougall. Trap design for insertable second-nuclei radiofrequency coils for magnetic resonance imaging and spectroscopy. *Concepts in Magnetic Resonance Part B: Magnetic Resonance Engineering*, 35B(3):121–132, 2009.

[10] Linda S. de Vries and Floris Groenendaal. Patterns of neonatal hypoxic–ischaemic brain injury. *Neuroradiology*, 52(6):555–566, June 2010. PMID: 20390260 PMCID: PMC2872019.

[11] Donna A. Goff, Erin M. Buckley, Turgut Durduran, Jiongjong Wang, and Daniel J. Licht. Noninvasive cerebral perfusion imaging in high-risk neonates. *Seminars in perinatology*, 34(1):46–56, February 2010. PMID: 20109972 PMCID: PMC2829712.

[12] E. Mark Haacke, Robert W. Brown, Michael R. Thompson, and Ramesh Venkatesan. *Magnetic Resonance Imaging: Physical Principles and Sequence Design*. Wiley, June 1999.

[13] Henrik Hagberg, Rebecca Ichord, Charles Palmer, Jerome Y Yager, and Susan J Vannucci. Animal models of developmental brain injury: relevance to human disease. a summary of the panel discussion from the third hershey conference on developmental cerebral blood flow and metabolism. *Developmental neuroscience*, 24(5):364–366, 2002. PMID: 12640174.

[14] Brian Hicks and Bill Erickson. Bias-t design considerations for the LWA, 2008.

[15] S K Hilal, A A Maudsley, H E Simon, W H Perman, J Bonn, M E Mawad, A J Silver, S R Ganti, P Sane, and I C Chien. In vivo NMR imaging of tissue sodium in the intact cat before and after acute cerebral stroke. *AJNR. American journal of neuroradiology*, 4(3):245–249, June 1983. PMID: 6410713.

[16] D.I Hoult and R.E Richards. The signal-to-noise ratio of the nuclear magnetic resonance experiment. *Journal of Magnetic Resonance (1969)*, 24(1):71–85, October 1976.

[17] S. Jarrix, T. Dubois, R. Adam, P. Nouvel, B. Azais, and D. Gasquet. Probe characterization for electromagnetic near-field studies. *IEEE Transactions on Instrumentation and Measurement*, 59(2):292–300, 2010.

[18] J. W. jr Jewett and Raymond A. Serway. *Physics for Scientists and Engineers with Modern Physics*. Cengage Learning EMEA, 2008.

[19] Ivo Juránek and Ladislav Bačiak. Cerebral hypoxia–ischemia: Focus on the use of magnetic resonance imaging and spectroscopy in research on animals. *Neurochemistry International*, 54(8):471–480, July 2009.

[20] V D Kodibagkar and M S Conradi. Remote tuning of NMR probe circuits. *Journal of magnetic resonance (San Diego, Calif.: 1997)*, 144(1):53–57, May 2000. PMID: 10783273.

[21] Vadim Kuperman. *Magnetic Resonance Imaging: Physical Principles and Applications*. Academic Press, 2000.

[22] George C. LaVerde, Charles A. Jungreis, Edwin Nemoto, and Fernando E. Boada. Sodium time course using 23Na MRI in reversible focal brain ischemia in the monkey. *Journal of Magnetic Resonance Imaging*, 30(1):219–223, 2009.

[23] M I Levene. The role of NMR and other techniques in neonatal imaging. *Journal of perinatal medicine*, 13(6):259–264, 1985. PMID: 4087116.

[24] Yang-Kang Li, Guo-Rui Liu, Xiu-Guo Zhou, and Ai-Qun Cai. Experimental hypoxic–ischemic encephalopathy: comparison of apparent diffusion coefficients and proton magnetic resonance spectroscopy. *Magnetic Resonance Imaging*, 28(4):487–494, May 2010.

[25] Gregory A Lodygensky, Terrie E Inder, and Jeffrey J Neil. Application of magnetic resonance imaging in animal models of perinatal hypoxic-ischemic cerebral injury. *International journal of developmental neuroscience: the official journal of the International Society for Developmental Neuroscience*, 26(1):13–25, February 2008. PMID: 17977687.

[26] E. Martin and A. J. Barkovich. Magnetic resonance imaging in perinatal asphyxia. *Archives of Disease in Childhood. Fetal and Neonatal Edition*, 72(1):F62–F70, January 1995. PMID: 7743289 PMCID: PMC2528424.

[27] William McGuire. Perinatal asphyxia. *Clinical Evidence*, 2007, November 2007. PMID: 19450354 PMCID: PMC2943784.

[28] Donald W. McRobbie. *MRI from Picture to Proton*. Cambridge University Press, 2007.

[29] Joël Mispelter, Mihaela Lupu, and André Briguet. *Nmr Probeheads for Biophysical And Biomedical Experiments: Theoretical Principles And Practical Guidelines*. Imperial College Press, 2006.

[30] M E Moseley, W M Chew, M C Nishimura, T L Richards, J Murphy-Boesch, G B Young, T M Marschner, L H Pitts, and T L James. In vivo sodium-23 magnetic resonance surface coil imaging: observing experimental cerebral ischemia in the rat. *Magnetic resonance imaging*, 3(4):383–387, 1985. PMID: 4088012.

[31] B. H. Munkeby, C. De Lange, K. E. Emblem, A. Bjørnerud, G. A. B. Kro, J. Andresen, E. H. Winther-Larssen, E. M. Løberg, and J. K. Hald. A piglet model for detection of hypoxic-ischemic brain injury with magnetic resonance imaging. *Acta Radiologica (Stockholm, Sweden : 1987)*, 49(9):1049–1057, October 2008. PMID: 18720081 PMCID: PMC2582156.

[32] A Nalin, G Frigieri, P Caggia, and S Vezzalini. State of the art of magnetic resonance (MR) in neonatal hypoxic-ischemic encephalopathy. *Child's nervous system: ChNS: official journal of the International Society for Pediatric Neurosurgery*, 5(6):350–355, December 1989. PMID: 2692812.

[33] Frances J Northington. Brief update on animal models of hypoxic-ischemic encephalopathy and neonatal stroke. *ILAR journal / National Research Council, Institute of Laboratory Animal Resources*, 47(1):32–38, 2006. PMID: 16391429.

[34] Aaron Oliver-Taylor. *Parallel Transmission Methods for Arterial Spin Labelling Magnetic Resonance Imaging*. PhD thesis, UCL, 2012.

[35] Ronald Ouwerkerk. Sodium magnetic resonance imaging: From research to clinical use. *Journal of the American College of Radiology*, 4(10):739–741, October 2007.

[36] E T Petersen, I Zimine, Y-C L Ho, and X Golay. Non-invasive measurement of perfusion: a critical review of arterial spin labelling techniques. *The British journal of radiology*, 79(944):688–701, August 2006. PMID: 16861326.

[37] Rudolph Pienaar, Michael J. Paldino, Neel Madan, Kalpathy S. Krishnamoorthy, David C. Alsop, Mathieu Dehaes, and P. Ellen Grant. A quantitative method for correlating observations of decreased apparent diffusion coefficient with elevated cerebral blood perfusion in newborns presenting cerebral ischemic insults. *NeuroImage*, 63(3):1510–1518, November 2012.

[38] Pierre-Marie Robitaille and Lawrence Jules Berliner. *Ultra High Field Magnetic Resonance Imaging*. Springer, January 2006.

[39] Victor D Schepkin, William W Brey, Peter L Gor'kov, and Samuel C Grant. Initial in vivo rodent sodium and proton MR imaging at 21.1 t. *Magnetic resonance imaging*, 28(3):400–407, April 2010. PMID: 20045599.

[40] Lina Shalak and Jeffrey M. Perlman. Hypoxic–ischemic brain injury in the term infant-current concepts. *Early Human Development*, 80(2):125–141, November 2004.

[41] Rakesh Sharma. Contrast enhancement methods in sodium MR imaging: a new emerging technique. *Journal of Biomedical Science and Engineering*, 02(06):445–457, 2009.

[42] Christopher H. Sotak. The role of diffusion tensor imaging in the evaluation of ischemic brain injury – a review. *NMR in Biomedicine*, 15(7-8):561–569, 2002.

[43] Günter Steidle, Hansjörg Graf, and Fritz Schick. Sodium 3-d MRI of the human torso using a volume coil. *Magnetic Resonance Imaging*, 22(2):171–180, February 2004.

[44] Agilent Technologies. Understanding the fundamental principles of vector network analysis, 2012.

[45] J.S. Thornton, R.J. Ordidge, J. Penrice, E.B. Cady, P.N. Amess, S. Punwani, M. Clemence, and J.S. Wyatt. Anisotropic water diffusion in white and gray matter of the neonatal piglet brain before and after transient hypoxia-ischaemia. *Magnetic Resonance Imaging*, 15(4):433–440, 1997.

[46] J. Thomas Vaughan and John R. Griffiths. *RF Coils for MRI*. John Wiley & Sons, December 2012.

[47] R J Vermeulen, W P F Fetter, L Hendrikx, P E M Van Schie, M S van der Knaap, and F Barkhof. Diffusion-weighted MRI in severe neonatal hypoxic ischaemia: the white cerebrum. *Neuropediatrics*, 34(2):72–76, April 2003. PMID: 12776227.

[48] F. Vial, S. Serriere, L. Barantin, J. Montharu, L. Nadal-Desbarats, L. Pourcelot, and F. Seguin. A newborn piglet study of moderate hypoxic-ischemic brain injury by 1H-MRS and MRI. *Magnetic Resonance Imaging*, 22(4):457–465, May 2004.

[49] J.H Walton and Mark S Conradi. Probe tuning adjustments—Need they be in the probe? *Journal of Magnetic Resonance (1969)*, 81(3):623–627, February 1989.

[50] Jiongjiong Wang and Daniel J. Licht. Pediatric perfusion MR imaging using arterial spin labeling. *Neuroimaging Clinics of North America*, 16(1):149–167, February 2006.

[51] Jiongjiong Wang, Daniel J Licht, Geon-Ho Jahng, Chia-Shang Liu, Joan T Rubin, John Haselgrove, Robert A Zimmerman, and John A Detre. Pediatric perfusion imaging using pulsed arterial spin labeling. *Journal of magnetic resonance imaging: JMRI*, 18(4):404–413, October 2003. PMID: 14508776.

[52] Friedrich Wetterling, Miroslav Högler, Ute Molkenthin, Sven Junge, Lindsay Gallagher, I. Mhairi Macrae, and Andrew J. Fagan. The design of a double-tuned two-port surface resonator and its application to in vivo hydrogen- and sodium-MRI. *Journal of Magnetic Resonance*, 217(0):10–18, April 2012.

[53] Dustin D. Wheeler and Mark S. Conradi. Practical exercises for learning to construct NMR/MRI probe circuits. *Concepts in Magnetic Resonance Part A*, 40A(1):1–13, 2012.

[54] P. Wintermark, A. Hansen, M. C. Gregas, J. Soul, M. Labrecque, R. L. Robertson, and S. K. Warfield. Brain perfusion in asphyxiated newborns treated with therapeutic hypothermia. *American Journal of Neuroradiology*, 32(11):2023–2029, December 2011.

[55] Ronald L. Wolf and John A. Detre. Clinical neuroimaging using arterial spin-labeled perfusion MRI. *Neurotherapeutics : the journal of the American Society for Experimental NeuroTherapeutics*, 4(3):346–359, July 2007. PMID: 17599701 PMCID: PMC2031222.